JOURNAL OF BACTERIOLOGY, June 2007, p. 3996–4013 Vol. 189, No. 11
0021-9193/07/$08.00+0 doi:10.1128/JB.00185-07

The Global Transcriptional Responses of *Bacillus anthracis* Sterne ($34F_2$) and a Δ*sodA1* Mutant to Paraquat Reveal Metal Ion Homeostasis Imbalances during Endogenous Superoxide Stress▽†

Karla D. Passalacqua,[1] Nicholas H. Bergman,[1,2] Jung Yeop Lee,[3] David H. Sherman,[1,3] and Philip C. Hanna[1]*

Department of Microbiology and Immunology,[1] Bioinformatics Program, University of Michigan Medical School,[2] and Life Sciences Institute and Department of Medicinal Chemistry,[3] University of Michigan, Ann Arbor, Michigan 48109

Received 4 February 2007/Accepted 12 March 2007

Microarray analyses were conducted to evaluate the paraquat-induced global transcriptional response of *Bacillus anthracis* Sterne ($34F_2$) to varying levels of endogenous superoxide stress. Data revealed that the transcription of genes putatively involved in metal/ion transport, bacillibactin siderophore biosynthesis, the glyoxalase pathway, and oxidoreductase activity was perturbed most significantly. A *B. anthracis* mutant lacking the superoxide dismutase gene *sodA1* (Δ*sodA1*) had transcriptional responses to paraquat similar to, but notably larger than, those of the isogenic parental strain. A small, unique set of genes was found to be differentially expressed in the Δ*sodA1* mutant relative to the parental strain during growth in rich broth independently of induced oxidative stress. The bacillibactin siderophore biosynthetic genes were notably overexpressed in Sterne and Δ*sodA1* cells after treatment with paraquat. The bacillibactin siderophore itself was isolated from the supernatants and lysates of cells grown in iron-depleted medium and was detected at lower levels after treatment with paraquat. This suggests that, while transcriptional regulation of these genes is sensitive to changes in the redox environment, additional levels of posttranscriptional control may exist for bacillibactin biosynthesis, or the enzymatic siderophore pipeline may be compromised by intracellular superoxide stress or damage. The Δ*sodA1* mutant showed slower growth in a chelated iron-limiting medium but not in a metal-depleted medium, suggesting a connection between the intracellular redox state and iron/metal ion acquisition in *B. anthracis*. A double mutant lacking both the *sodA1* and *sodA2* genes (Δ*sodA1* Δ*sodA2*) was attenuated for growth in manganese-depleted medium, suggesting a slight level of redundancy between *sodA1* and *sodA2*, and a role for the *sod* genes in manganese homeostasis.

Bacillus anthracis initiates infection by entering the host in one form, as a dormant endospore, and establishing the disease anthrax in an entirely different form, as the vegetative bacillus (21). In order for *B. anthracis* to make the transition from endospore to bacillus, the microbe must be able to adapt rapidly to a variety of environmental conditions presented within a host. Pathogenic bacteria have evolved various mechanisms for rapid adaptation to life inside a host, where they encounter a variety of environmental pressures. One way to explore the many survival strategies of pathogenic bacteria is to study the transcriptional responses to various insults in vitro that mimic conditions that may be confronted in vivo. Classic stress conditions include starvation, heat, cold, ionizing radiation, osmolarity, nutrient limitation, pH, and oxidation-reduction (redox) (6, 30, 36, 57, 68, 70, 76). The environments actually encountered by bacteria during infection are most likely a subtle and complex mixture of various stresses; however, studying each response separately helps provide insight into how responses are conserved relative to those of nonpathogenic model organisms such as *Escherichia coli* and *Bacillus subtilis* and may reveal unique mechanisms that have evolved to support various pathogenic lifestyles.

Changes in the intracellular and extracellular redox environment can affect cells by altering or damaging biomolecules (20). Reactive metabolites such as hydrogen peroxide and superoxide are normal intracellular by-products of aerobic metabolism, and conserved molecular mechanisms such as the scavenging enzymes catalase and superoxide dismutase (SOD) are present in aerobic organisms for protection from these endogenously produced oxidatively active species (18, 42, 46). Because these metabolites are unique in their chemical properties, cellular transcriptional responses to them are often distinctive. Additionally, reactive molecules such as superoxide and nitric oxide are ubiquitous signaling molecules in eukaryotic systems (3, 28, 29). During the establishment and progression of anthrax, reactive oxygen metabolites may be encountered by *B. anthracis* exogenously, such as from the oxidative burst of phagocytic cells of the innate immune system (19, 35, 59) and in the extracellular milieu established in certain tissues of a host (34, 47, 75). Since superoxide is a charged radical, it is not diffusible across membranes, and the exogenous encounter with this reactive oxygen metabolite presumably would not affect a transcriptional program (24). However, when bacteria are growing rapidly and to very high titers within the host during late infection, they are presumably generating metabolic by-products of their own (63) and, depending on the

* Corresponding author. Mailing address: Department of Microbiology and Immunology, University of Michigan Medical School, 1150 West Medical Center Dr., 6703 Medical Science Building II, Box 0620, Ann Arbor, MI 48109. Phone: (734) 615-3706. Fax: (734) 764-3562. E-mail: pchanna@umich.edu.

† Supplemental material for this article may be found at http://jb.asm.org/.

▽ Published ahead of print on 23 March 2007.

TABLE 1. Bacterial strains and plasmids used in this study

Strain or plasmid	Relevant phenotype	Reference or origin
Strains		
Bacillus anthracis		
Sterne $34F_2$	$pXO1^+$ $pXO2^-$	74
KDC3	$34F_2$ Δ*sodA1*::Km^r	62
KDC5	$34F_2$ Δ*sodA2*::Km^r	62
KDC7	$34F_2$ Δ*bac12345*	This work[a]
KDC8	$34F_2$ Δ*sodA1*::Km^r Δ*sodA2*	This work[a]
BA850	$34F_2$ Δ*asbABCDEF*	B. Janes
KDC8CA1	$34F_2$ Δ*sodA1*::Km^r Δ*sodA2*; pBKJ258A1	This work[a]
KDC8CA2	$34F_2$ Δ*sodA1*::Km^r Δ*sodA2*; pBKJ258A2	This work[a]
KDC3CA1	$34F_2$ Δ*sodA1*::Km^r; pBKJ258A1	62
Escherichia coli		
DH5α	F^- ϕ80*lacZ*Δ*M15* Δ(*lacZYA-argF*)*U169 recA1 endA1 hsdR17*(r_K^- m_K^+) *phoA supE44 thi-1 gyrA96 relA1* λ^-	Invitrogen
One Shot TOP10	F^- *mcrA* Δ(*mrr-hsdRMS-mcrBC*) ϕ80*lacZ*Δ*M15* Δ*lacX74 recA1 araD139* Δ(*ara-leu*)*7697 galU galK rpsL* (Str^r) *endA1 nupG*	Invitrogen
INV110	F′ {*tra*Δ*36 proAB lacI*^{q} *lacZ*Δ*M15*} *rpsL* (Str^r) *thr leu endA thi-1 lacY galK galT ara tonA tsx dam dcm supE44* Δ(*lac-proAB*) Δ(*mcrC-mrr*)*102*::Tn*10* (Tet^r)	Invitrogen
Plasmids		
pBKJ258	Erm^r	B. Janes
pBKJ223	Tet^r	B. Janes

[a] The TIGR Comprehensive Microbial Resource genome sequence for the virulent *Bacillus anthracis* Ames Ancestor strain was used for the creation of strains in this study. Therefore, GBAA numbers referenced are from the Ames Ancestor sequence.

mode of central metabolism, will need to adjust the transcriptional program to support optimal growth.

In this study, we used custom *Bacillus anthracis* Affymetrix GeneChips (4) to define and compare the global transcriptional responses of *B. anthracis* Sterne ($34F_2$) and an isogenic mutant lacking the SOD gene *sodA1* (Δ*sodA1*) to endogenous superoxide stress induced by the superoxide-generating compound paraquat. The *sodA1* gene has recently been shown to be necessary for protection from this type of oxidative stress (62), and the comparison of the responses of Sterne and the Δ*sodA1* mutant after this major physiological redox perturbation identified a transcriptional program involving genes for metal ion transport, siderophore biosynthesis, putative glyoxalase enzymes, and oxidoreductase activity. The substantial increase in the transcription of the genes involved in the biosynthesis of the iron-chelating siderophore bacillibactin after paraquat treatment led us to quantify extracellular and intracellular levels of both of the siderophores produced by *B. anthracis* (bacillibactin and petrobactin) in order to determine how siderophore production is influenced by oxidative stress. Because the transcriptional program after endogenous superoxide stress suggests a metal ion imbalance, the growth of the Δ*sodA1* and Δ*sodA2* mutants and of the Δ*sodA1* Δ*sodA2* double mutant in various types of metal-limiting media was also explored.

MATERIALS AND METHODS

Bacterial strains. The bacterial strains used in this study are listed in Table 1. The creation of Δ*sod*, Δ*asb*, and Δ*bac* mutants has been described previously (45, 62) All were constructed using the Sterne $34F_2$ parental strain. Spores of all strains were prepared in modified G medium as described previously (62). When antibiotics were used, concentrations for *B. anthracis* strains were 30 μg/ml for kanamycin and 5 μg/ml for erythromycin.

Cell growth conditions and RNA extraction. For RNA collection, overnight Luria-Bertani (LB) broth cultures of *Bacillus anthracis* strain Sterne ($34F_2$) and/or the Δ*sodA1* strain were diluted 1:100 into fresh LB medium in the morning and allowed to recover for approximately 2 h. Cells were back-diluted to an optical density at 600 nm(OD_{600}) of 0.01 in an 80-ml volume of fresh LB medium. Cells were allowed to grow to an OD_{600} of 0.4 to 0.5. The cultures were split into three separate 20-ml cultures, and methyl viologen (paraquat) (Aldrich 856177) was added to two of the flasks to a final concentration of 100 μM or 800 μM. The third flask was left untreated as a control. Cultures were allowed to grow for approximately 20 to 25 min. A 6-ml volume of cells was collected from each culture and pelleted by centrifugation at 4°C for 7 min at ~2,000 rpm. RNA was isolated using the Ambion RiboPure-Bacteria kit according to the manufacturer's instructions with the following modifications: cell disruption with zirconia beads was done for 15 min, 400 μl of RNAwiz reagent was used, BCP phase separation reagent was used in place of chloroform, and 50 μl of RNase- and DNase-free distilled water was added during extraction to optimize the yield. The QIAGEN RNeasy minikit with an on-column DNase digestion step was used according to the manufacturer's RNA cleanup protocol. RNA was quantified via the A_{260}:A_{280} ratio on a Beckman DU530 spectrophotometer. RNA integrity was checked using an Agilent 2100 bioanalyzer at the University of Michigan Affymetrix cDNA core facility. The procedures described above were carried out in three independent experiments utilizing unique spore starter cultures each time.

Microarray sample processing and data collection. RNA samples were reverse transcribed, and the corresponding cDNA samples were purified, fragmented, and labeled according to Affymetrix-recommended protocols (available at http://www.affymetrix.com/support/downloads/manuals/expression_s3_manual.pdf) at the University of Michigan Comprehensive Cancer Center microarray core facility. Hybridization to the *B. anthracis* GeneChips (4), as well as scanning of the arrays, was also done according to standard Affymetrix protocols. At this point, several quality control steps were performed in order to ensure that the raw data were of sufficient quality to proceed. First, the distributions of perfect-match probe intensities for each chip were compared, since the robust-multichip-average procedure used for normalization and background correction over multiple chips is based on the assumption that these distributions are very similar. Then, a plot of average probe intensity versus position within a gene was generated for each sample. This plot shows if there are systematic skews within a given data set toward probes that lie near the end of each gene, which would indicate a high level of RNA degradation or problems with the reverse transcription (RT) step. Once it was verified that all the samples showed similar 5′-to-3′ profiles, the

robust-multichip-average method was used to subtract background, normalize data, and compute a single probe set summary for each gene (8, 43, 44). Principal-component analysis verified that biological replicates were very similar to each other and formed relatively tight clusters (data not shown).

Microarray data analysis. Significance analysis of microarrays (SAM) was performed using the TMeV 3.1 (version 10.2) suite of programs (http://www.tm4.org/) (68a). Note that in all cases, SAM were done with a false discovery rate of <0.001. Pathway analysis of array data was done using the EASE algorithm (39) as implemented within the TM3-MeV program, as well as a set of GO and TIGRFAM tables compiled from the TIGR Comprehensive Microbial Resource (http://www.tigr.org/CMR/). The significance of overrepresentations was assessed using the Fisher exact text. Note that only those genes that showed statistically significant up- or down-regulation and at least a twofold change in expression are listed in the tables and in the supplemental material.

Assays of growth under iron- and manganese-limiting conditions. Growth curves assessing the growth of *B. anthracis* strains in media containing the iron chelator 2,2′-dipyridyl and in media predepleted of cations were performed as follows. For chelated medium, LB medium alone or with 300 μM or 400 μM 2,2′-dipyridyl was dispensed in 100-μl volumes into flat-bottom, 96-well tissue culture-treated polystyrene plates (Corning-Costar 3628). The vegetative bacilli of the strains indicated were grown to mid-exponential phase (OD_{600}, ~0.4 to 0.5), washed three times in sterile metal-depleted medium, and then back-diluted to an OD_{600} of approximately 0.08 to 0.10. Culture growth was assessed in a Molecular Devices Spectramax M2 spectrophotometer for 10 to 12 h at 37°C; A_{600} readings were taken every 10 min, with shaking for 560 s (~9.3 min) between readings. For depleted medium, experiments were performed as for chelated medium but with iron- and manganese-depleted medium (IMnDM), with or without addition of $Fe(II)SO_4 \cdot 7H_2O$ or $MnSO_4 \cdot H_2O$ to a final concentration of 20 μM each. IMnDM was prepared like iron-depleted medium (IDM) (as reported previously [13]) but without the addition of manganese salts. Cations were depleted by using Bio-Rad Chelex 100.

Doubling times were calculated as follows, according to the method of Moat et al. (56). First, the variable n was calculated as $[\log_{10}(\text{high } OD_{600}) - \log_{10}(\text{low } OD_{600})]/0.3010$, where OD_{600} values are from exponentially dividing cells. Then the doubling time was calculated as [time (in minutes) between the high OD_{600} and the low OD_{600}]/n.

The MIC of 2,2′-dipyridyl for spore outgrowth was determined as follows. LB medium with 0, 100, 200, 300, 400, and 500 μM 2,2′-dipyridyl was prepared and distributed in 100-μl volumes in flat-bottom 96-well tissue culture-treated polystyrene plates (Corning-Costar 3628). Approximately 10^5 spores of each strain were added to each well (three separate strain stocks in three separate experiments). Outgrowth was assessed as the ability to establish exponential growth to an OD_{600} of at least 0.3 after 8 h of incubation at 37°C in a Molecular Devices Spectramax M2 spectrophotometer, with A_{600} readings taken every 10 min and with shaking for 560 s (~9.3 min) between readings.

End point RT-PCR. A total of 700 ng of RNA collected from *B. anthracis* Sterne ($34F_2$) and the Δ*sodA1* mutant (as described above) was used to perform end point RT-PCR using Invitrogen one-step RT-PCR with Platinum *Taq* according to the manufacturer's instructions. Briefly, RT was performed at 50°C for 30 min. PCR was performed with 0.25 pg of operon- or gene-specific primers (sequences available upon request) for 37 cycles with an elongation temperature of 70°C and an extension time of 30 s. Five microliters of each PCR product was run on a 0.7% Tris-borate-EDTA agarose gel and visualized by ethidium bromide staining. Negative controls omitting reverse transcriptase and positive controls with *B. anthracis* Sterne ($34F_2$) and Δ*sodA1* genomic DNAs were run with each experiment and primer pair. Operon- or gene specific primers were designed to result in products of approximately 200 bp.

SYBR green quantitative RT-PCR. RNA was collected from Sterne and Δ*sodA1* cells as described above. A total of 700 ng of RNA was used to make cDNA using 300 ng of random primers and Invitrogen SuperScript II reverse transcriptase, by following the maker's protocol, with an overnight incubation at 42°C. For all samples, a control without reverse transcriptase was performed. Diagnostic PCR of the cDNA was done using 1.5 μl of each reaction product to eliminate the possibility of genomic DNA contamination (all results were negative) and for the confirmation of DNA synthesis using primers for the *fusA* gene.

SYBR green PCR was performed on an ABI Prism 7900HT system at the University of Michigan cDNA Affymetrix core facility at the Comprehensive Cancer Center. The Applied Biosystems SYBR green master mix was used with 1.5 μl of the cDNA preparations. Each reaction was performed twice with two biological replicates, for a total of four reactions per gene-specific primer pair per condition (with cDNA, without cDNA, and without reverse transcriptase). Forty elongation cycles were performed with 30-s elongation times and an annealing temperature of 55°C (optimized beforehand), with a melting temperature of 94°C and an extension temperature of 68°C.

Gene-specific primers used corresponded to overlapping segments of the first two genes in the *bac* operon (GBAA2369 and -2370) and internal segments of the following genes: the second gene in the *asb* operon (GBAA1982), the gene encoding the glyoxalase family protein (GBAA3339), the *ccdA-1* cytochrome *c*-type biogenesis protein gene (GBAA1778), the thioredoxin family protein gene (GBAA1779), and the prolipoprotein diacylglyceryl transferase family protein gene (GBAA1780). (All PCR products were between 180 and 200 bp. Primer sequences are available upon request).

Threshold cycle (C_T) values are the values where the PCR enters exponential amplification. Approximate transcript abundance was analyzed using the comparative C_T method (or $2^{-\Delta\Delta C_T}$ method). The C_T for the *fusA* control PCR product is subtracted from each of the experimental C_Ts. The difference in transcript abundance is then calculated as $2^{-(\text{difference in normalized } C_T\text{s})}$. C_Ts used are averages for four reactions.

Quantification of the siderophores bacillibactin and petrobactin. Three-milliliter overnight cultures of *B. anthracis* Sterne $34F_2$ and the Δ*sodA1* and Δ*bac* mutants were added to 100 ml of LB medium or IDM (13) in 500-ml plastic flasks. At an OD_{600} of approximately 0.4 to 0.5, paraquat (methyl viologen) was added to a final concentration of 800 μM. Cultures were incubated for 1 h at 37°C with shaking at 300 rpm. Supernatants were collected via filtration with Corning 0.2-μm-pore-size vacuum filter flasks.

For cell lysates, cells from filter flasks were resuspended in 20 ml of sterile phosphate-buffered saline, pH 7.4 (without calcium chloride or magnesium chloride). Cells were freeze-thawed three times, once at −20°C and twice at −80°C. Cell suspensions were sonicated six times with 30-s pulses at 4°C. Cell lysates were pelleted by centrifugation, and lysate supernatants were incubated on ice with 18 μl of DNase (RNase free) (180 U) for 1 h. Lysates were then spun by centrifugation at 9,000 × *g* for 35 min, and lysate supernatants were collected for analysis. Total protein concentrations were assayed using the Qubit protein assay (Molecular Probes).

For quantification of bacillibactin, cytosolic fractions (5 ml) from LB or IDM cultures were adjusted to pH 2.0 and then extracted three times with equal volumes of ethyl acetate. The organic layers were pooled, and the solvents were concentrated into dryness in vacuo. The dried pellets were dissolved in 50 μl of methanol and used for quantitative analysis of intracellular bacillibactin. Samples were prepared for quantification of extracellular bacillibactin by extracting acidified (pH 2.0) LB or IDM culture supernatants (10 ml) with an equal volume of ethyl acetate three times. Organic fractions were pooled and concentrated into 100 μl of methanol for analysis.

For quantification of petrobactin, cytosolic fractions (5 ml) or supernatants (10 ml) from LB or IDM cultures were adjusted to pH 7.0. XAD-16 resin was added (1 g for the cytosolic fraction, 2 g for supernatants), and the mixtures were shaken for 1 h at 150 rpm in the dark. Mixtures were then filtered, the resin was washed with pure water three times, and extracts were eluted with methanol (5 ml for the cytosolic fraction and 10 ml for supernatants). Methanol eluates were concentrated to dryness in vacuo and dissolved in 50 μl (cytosolic) or 100 μl (supernatant) of 80% methanol for quantification.

The organic solvent or XAD-16 resin extracts from the culture supernatants or cytosolic fractions of *B. anthracis* were analyzed using a Shimadzu LCMS-2010EV system. (The liquid chromatography-mass spectrometry [LC-MS] analysis is described in detail in the next section.) 2,3-Dihydroxybenzoic acid (for bacillibactin) and 3,4-dihydroxybenzoic acid (for petrobactin) were utilized as internal standards for signal normalization. Ten microliters of a 2,3-dihydroxybenzoic acid or 3,4-dihydroxybenzoic acid stock solution (1 mM) was added to 100 μl of each sample. By the LC methods described below, bacillibactin and 2,3-dihydroxybenzoic acid showed retention times of 19.230 to 19.340 and 17.367 min, and petrobactin and 3,4-dihydroxybenzoic acid showed retention times of 15.860 to 16.134 and 18.133 min, respectively. The calibration curves were constructed by using a series of 10 concentrations (ranging from 10 to 500 μM) of authentic bacillibactin and petrobactin for quantification. The retention time and mass spectrum of the corresponding bacillibactin or petrobactin peak in each sample were compared with those of authentic bacillibactin or petrobactin standards. The intracellular bacillibactin and petrobactin quantities were calculated in μg/mg of cell protein. The extracellular bacillibactin and petrobactin concentrations were calculated in μg/ml of culture supernatant. Quantifications were performed three times for each extract, and means and standard deviations were calculated form the total data set.

LC-MS analysis. LC was performed on a Shimadzu LC-20AD high-performance liquid chromatography (HPLC) system consisting of a UV/visible detector (SDP-20AV) and an autosampler (SIL-20AC). The HPLC was coupled to a Shimadzu LCMS-2010EV mass spectrometer with an electrospray ionization

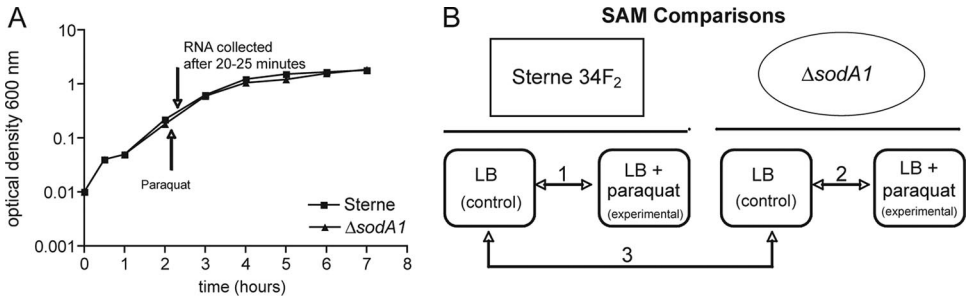

FIG. 1. Outline of experiments for microarray analysis of the transcriptional response of *B. anthracis* to paraquat. (A) Representative growth curves of *B. anthracis* Sterne $34F_2$ and the Δ*sodA1* mutant in rich LB medium. During logarithmic growth (OD_{600}, ~0.4 to 0.5), cultures were split into three, and paraquat was added to two flasks at 100 μM and 800 μM. Cells were allowed to grow for ~20 to 25 min, and RNA was collected as described in Materials and Methods. (B) Schematic of SAM discussed in the text, comparing differentially expressed genes under various growth conditions as indicated by arrows. Comparisons are as follows: 1, genes over- or underexpressed in Sterne treated with paraquat relative to Sterne growing in untreated LB; 2, genes over- or underexpressed in the Δ*sodA1* mutant treated with paraquat relative to the Δ*sodA1* mutant growing in untreated LB; 3, genes over- or underexpressed in the Δ*sodA1* mutant growing in untreated LB relative to the parental strain, Sterne, growing in untreated LB.

interface. LC was carried out on an analytical column (Waters XBridge C_{18}; particle size, 3.5 μm; column dimensions, 2.1 by 150 mm) using a linear stepwise gradient from 10% to 100% aqueous acetonitrile in 0.1% (vol/vol) formic acid at a flow rate of 0.1 ml/min over 30 min for intra- and extracellular bacillibactin analysis. Solvent systems with a gradient from 5% to 50% aqueous acetonitrile in 0.1% (vol/vol) formic acid over 30 min were used for intra- and extracellular petrobactin analysis under the LC conditions described above. The electrospray ionization source was set at the positive mode. Selected ion monitoring (SIM) was conducted to monitor ions at *m/z* 883.2, 719.3, and 155.2, which corresponded to the protonated molecular ions of bacillibactin, petrobactin, and internal standards 2,3-dihydroxybenzoic acid and 3,4-dihydroxybenzoic acid, respectively. The MS operating conditions were optimized as follows: drying gas flow rate, 0.1 ml/min; curved desolvation line temperature, 250°C; heat block temperature, 200°C; detector voltage, 1.5 kV.

Methylglyoxal sensitivity assays. (i) MIC. Sterne cells were grown in LB medium to an OD_{600} of ~0.5 and back-diluted to an OD_{600} of 0.01 into fresh medium containing 0, 100, 200, 300, or 500 μM methylglyoxal (Sigma M0252). Cells were allowed to grow overnight and were scored for growth versus no growth.

(ii) Disk diffusion assay. Two separate *B. anthracis* Sterne cultures were grown in LB medium to an OD_{600} of 0.7 to 0.9, and each culture was diluted 1:2 into fresh medium twice. Paraquat was added to a final concentration of 800 μM to one of each set of biological samples. Cells were grown at 37°C with shaking at 300 rpm for 45 min. Cultures were diluted 1:10 into phosphate-buffered saline, and 200 μl was spread as a lawn onto brain heart infusion agar plates. Plates were allowed to dry for 30 min, and two disks infused with 10 μl of 20% methylglyoxal were placed on each plate. H_2O was used as a negative control. Plates were incubated overnight at 37°C, and zones were measured independently by two investigators in the morning. Averages were calculated for 20 disks total for each treatment (LB medium alone versus LB medium plus paraquat). A two-tailed Student *t* test with unequal variance was performed on Excel 2004 for Mac and on Prism 4 for Mac.

Microarray data accession number. All microarray data described in this study are freely available in the ArrayExpress database (http://www.ebi.ac.uk/arrayexpress) under accession number E-MEXP-1043. The custom *B. anthracis* microarrays can be purchased from Affymetrix with permission from the developers (for research purposes); further information can be obtained by contacting the authors.

RESULTS AND DISCUSSION

Experimental design and layout of SAM comparisons. Previously, it was shown that of the four putative SODs encoded on the *B. anthracis* genome (*sodA1*, *sodA2*, *sodC*, and *sod15*), only *sodA1* was required for protection from endogenous superoxide stress, even though both SODA1 and SODA2 are enzymatically active proteins and have been shown to form an active heterodimer (62). Therefore, we sought to determine the genome-wide transcriptional changes in response to paraquat for wild-type *B. anthracis* (Sterne $34F_2$) and for the isogenic *sodA1* deletion mutant (Δ*sodA1*) in order to ascertain the character of the transcriptional program in response to a potentially toxic physiological perturbation of intracellular redox balance and to elucidate the impact of a lack of *sodA1* on transcriptional regulation during aerobic growth. Figure 1A shows typical growth curves of *B. anthracis* Sterne and the Δ*sodA1* mutant in rich LB broth, indicating that these two strains have identical growth kinetics when grown in rich medium. The transcriptional responses of other bacteria to various redox cycling reagents have been explored in a variety of ways, and approaches have differed widely in the amount of time for which a given organism is exposed to a given stress (e.g., 20 min, 30 min, 2 h, 15 min, or 10 to 20 min of exposure to H_2O_2, and 45 min of exposure to paraquat) (14, 15, 50, 64, 66, 69). We chose to collect RNA at 20 to 25 min after exposure to two different concentrations of paraquat (100 μM and 800 μM) for several reasons. First, we wanted to perform at least three biological replicates at two different concentrations; hence, considering the number of GeneChips needed for appropriate controls, RNA was collected at one time point. Second, the two paraquat concentrations represent both a low-end concentration that is entirely nontoxic to wild type *B. anthracis* and only mildly attenuating to the Δ*sodA1* mutant and an upper-end concentration that is toxic only to the Δ*sodA1* mutant, but not immediately so, such that quality RNA could still be isolated from this mutant and dose-dependent levels of transcriptional change might be seen (62). Last, *B. anthracis* has a doubling time of approximately 50 ± 10 min in LB medium (data not shown), and because two different concentrations of paraquat were to be compared, an incubation time equivalent to one-half the doubling time was chosen in order to reveal an overall global set of transcriptional differences after two levels of an intracellular physiological imbalance were established. Our goal here was not to define a canonical "regulon" but rather to determine a global transcriptional snapshot resulting from a perturbation in intracellular physiology for two strains that we presumed would respond to the stress uniquely. We performed three independent microarray exper-

TABLE 2. Functional family analysis of genes showing statistically significant, >2-fold changes in expression levels in exponentially growing Sterne and Δ*sodA1* strains after treatment with paraquat as outlined in Fig. 1

Functional family	No. of genes in overrepresented functional families that were differentially expressed in the following strain under the indicated conditions (*P* value)[a]:				
	Sterne		Δ*sodA1* mutant		
	With 100 μM PQ[b]	With 800 μM PQ	With 100 μM PQ	With 800 μM PQ	In LB only (compared to Sterne)
Higher-level expression					
Transport and binding proteins[c]	5 (3.19E-02)	13 (3.23E-03)	38 (1.16E-09)	44 (8.38E-12)	8 (1.88E-03)
Siderophore biosynthesis[d]	2 (6.649E-04)	5 (9.01E-08)	5 (2.59E-06)	6 (2.07E-07)	
Electron transport				5 (4.46E-02)	2 (4.07E-02)
Metabolism/catalytic activity[e]	4 (2.57E-03)	6 (1.45E-02)	9 (1.58E-02)	—[e]	4 (4.48E-02)
Riboflavin, FMN, and FAD				3 (3.82E-04)	
Fermentation		2 (3.93E-02)		3 (4.79E-02)	
Lower-level expression					
Proline biosynthesis					2 (3.37E-03)
Potassium ion transport					2 (1.03E-03)
ATPase activity coupled to transmembrane movement of substances					8 (1.25E-02)
Transport and binding proteins[c]		17 (1.29E-07)	5 (1.99E-02)	16 (2.09E-04)	
Purines, pyrimidines, nucleosides, and nucleotides		5 (1.48E-04)	4 (4.50E-05)	6 (1.02E-04)	
Chemotaxis[f]				2 (2.61E-02)	

[a] *P* values were determined using the Fisher exact test within EASE analysis (see Materials and Methods). All individual genes that are expressed at levels >2-fold higher or lower than those in control samples can be found either in Table 4 or in the tables in the supplemental material.

[b] PQ, paraquat.

[c] A very large and general category in the functional family tables used for these analyses. This aspect of *B. anthracis* biology is mainly uncharacterized at present. The more-specific, underlying trends for all strains and comparisons listed above are as follows: (i) transport and binding proteins exhibiting higher-level expression are mainly putative transporters of iron and potassium, general ABC transporters, drug resistance transporters, or major facilitator transporters; (ii) those exhibiting lower-level expression are mainly categorized as ABC and phosphate transporters, with various oligopeptide, formate, and nucleoside transporters as well.

[d] With one exception, the more highly expressed siderophore biosynthesis genes listed in this table are from the *bac*/bacillibactin biosynthetic cluster, as opposed to the virulence-associated *asb*/petrobactin biosynthetic cluster (13, 49).

[e] In all cases listed here, this functional family includes primarily glyoxalase family proteins, as well as the pyridine-nucleotide disulfide oxidoreductase family for the Δ*sodA1* mutant. Although this family, per se, is not listed in the Δ*sodA1* (800 μM paraquat) experimental group due to the *P* value cutoff, the genes themselves are up-regulated >2-fold in this group.

[f] Note that *B. anthracis* is a nonmotile organism.

iments for each condition utilizing three separate wild-type Sterne and Δ*sodA1* spore stock starter cultures in the absence (control) or presence (experimental) of two concentrations of paraquat (100 μM or 800 μM) (Fig. 1B) (62). Although it has been shown that the transcriptional responses to various redox cycling reagents can be rapid and differ over time (38, 80), the number of transcriptional differences we observe here show that after 20 to 25 min of exposure to paraquat, *B. anthracis* is undergoing an obvious transcriptional adjustment; however, we acknowledge that those genes whose transcription and RNA degradation both occur before 20 to 25 min of exposure will be missed (Fig. 1A).

Lists of genes expressed differentially by each experimental group versus its control group were generated using SAM as described in Materials and Methods (*B. anthracis* Affymetrix arrays with a total of 5,815 genes). Figure 1B schematically represents the SAM comparisons discussed below and is provided to serve as an aid to reading the data in Tables 2 and 3. The *B. anthracis* Affymetrix arrays were designed using the TIGR Ames Ancestor genome, a fully virulent strain. This laboratory uses the attenuated Sterne strain, and it should be noted that *B. anthracis* is an extremely monomorphic organism, with only slight genomic differences between strains (54). The microarrays were designed to be used for both fully virulent and attenuated strains; therefore, the pXO2 virulence plasmid, which is included on the GeneChip but is lacking in the Sterne strain, served as an additional and convenient negative control. Note that because of length considerations, the gene lists in Table 3 do not include hypothetical or conserved proteins and include only genes that show increased transcript abundance (≥2-fold). We are primarily interested in genes whose expression is induced by superoxide stress; however, all genes at least twofold differentially expressed, both up- and down-regulated, are listed in the tables in the supplemental material, arranged by TIGR gene number. Significantly overrepresented functional families were identified using the EASE algorithm as stated in Materials and Methods (39).

Comparison of genes differentially expressed in the Δ*sodA1* mutant relative to the parental Sterne strain during exponential growth in rich medium in the absence of induced oxidative stress. Because *sodA1* was found to be necessary for resistance to superoxide stress induced by the compounds paraquat and menadione (62), we hypothesize that this gene is important for the general maintenance of the redox status of the cell during normal aerobic growth in vitro, when superoxide is expected to be generated spontaneously during electron transport. Therefore, we compared genes differentially expressed by the Δ*sodA1* mutant relative to the wild-type parental strain during growth in rich medium without induced oxidative stress. SAM reveals that 25 genes are significantly overexpressed by the

TABLE 3. List of genes at least twofold differentially expressed in the *B. anthracis* Sterne and Δ*sodA1* strains after treatment with 100 or 800 μM paraquat[a]

Gene no. (*B. anthracis* Ames Ancestor genome)	Gene name and/or putative function[b]	Fold change in expression for the following comparison:				
		Sterne with LB plus paraquat vs LB alone (control)[c]		Δ*sodA1* mutant with LB plus paraquat vs LB alone (control)[d]		Δ*sodA1* mutant vs Sterne, both with LB alone[e]
		100 μM paraquat	800 μM paraquat	100 μM paraquat	800 μM paraquat	
Amino acid biosynthesis						
GBAA1808	*asnA*; aspartate–ammonia ligase			2.6	2.6	
GBAA4218	*metE*; 5-methyltetrahydropteroyltriglutamate–homocysteine methyltransferase				2.5	
Biosynthesis of cofactors, prosthetic groups, and carriers						
GBAA1158	*hemH-2*; ferrochelatase				3.1	
Cell envelope						
GBAA0781	Membrane protein, putative			2.7	2.0	
GBAA0837	Lipoprotein, putative			2.3	2.5	
GBAA1093	S-layer protein, putative			15.2	22.6	
GBAA1650	Membrane protein, putative		2.1			
GBAA1904	Membrane protein, putative					12.4
GBAA2638	Glycosyltransferase, putative	8.9	31.7	13.9	19.8	
GBAA3179	TspO/MBR family protein			4.5	4.1	
GBAA4738	Membrane protein, putative			2.5		
GBAA4746	Acid phosphatase					2.6
Cellular processes						
GBAA1159	*katB*; catalase		2.9	2.7		
GBAA1346	Internalin, putative			11.3	19.9	
GBAA5148	*comA* operon protein, putative			2.7	2.6	
GBAA5701	Channel protein, hemolysin III family		2.3			
Central intermediary metabolism						
GBAA2276	Azoreductase		2.6			
GBAA5561	Low-molecular-wt phosphotyrosine protein phosphatase family protein				2.5	
DNA replication, recombination, and repair						
GBAA1905	*topB-2*; DNA topoisomerase III					4.0
GBAA3180	Deoxyribodipyrimidine photolyase family protein				3.7	
Energy metabolism (amino acids and amines)						
GBAA1784	*dsdA*; D-serine dehydratase					2.0
Energy metabolism (electron transport)						
GBAA0838	NAD(P)H dehydrogenase, quinone family			3.1	3.2	
GBAA1394	Flavodoxin			18.5	36.4	
GBAA1778	*ccdA-1*; cytochrome *c*-type biogenesis protein CcdA					49.1
GBAA1779	Thioredoxin family protein					23.0
GBAA2113	*qor-1*; quinone oxidoreductase				5.0	
GBAA3544	*qor-2*; quinone oxidoreductase				2.2	
GBAA3596	Flavodoxin		5.5	35.8	46.5	
Energy metabolism (fermentation)						
GBAA0784	Alcohol dehydrogenase, zinc containing				2.1	
GBAA1296	*ywdH*; aldehyde dehydrogenase		2.2	3.2	2.7	
GBAA3438	Alcohol dehydrogenase, zinc containing		2.1		2.7	
Energy metabolism (pentose phosphate pathway)						
GBAA3432	*tkt-1*; transketolase		2.4		2.6	2.0
GBAA3433	*zwf*; glucose-6-phosphate 1-dehydrogenase				3.1	

Continued on following page

TABLE 3—*Continued*

Gene no. (*B. anthracis* Ames Ancestor genome)	Gene name and/or putative function[b]	Fold change in expression for the following comparison:				
		Sterne with LB plus paraquat vs LB alone (control)[c]		Δ*sodA1* mutant with LB plus paraquat vs LB alone (control)[d]		Δ*sodA1* mutant vs Sterne, both with LB alone[e]
		100 μM paraquat	800 μM paraquat	100 μM paraquat	800 μM paraquat	
Energy metabolism (photosynthesis)						
GBAA4255	Ribulose bisphosphate carboxylase, putative			2.6		
Enzymes of unknown specificity						
GBAA0352	Pyridine nucleotide-disulfide oxidoreductase family protein		2.1	4.4	5.6	2.6
GBAA0766	Nitroreductase family protein			16.2	20.3	
GBAA1110	Ser/Thr protein phosphatase family protein, authentic point mutation		2.5	4.0	3.5	
GBAA1217	Ser/Thr protein phosphatase family protein			3.6		
GBAA1361	Radical SAM domain protein		2.6			
GBAA1653	Glyoxalase family protein	37.2	85.4	50.2	54.1	
GBAA1780	Prolipoprotein diacylglyceryl transferase family protein					31.4
GBAA1865	Chlorohydrolase family protein	2.6	2.5			
GBAA2038	NADH:flavin oxidoreductase/NADH oxidase family protein			2.0	2.2	
GBAA2639	Aspartate racemase family protein		3.7			
GBAA3339	Glyoxalase family protein	3.3	28.2	6.9	8.0	
GBAA3595	BNR repeat domain protein		5.8	34.7	45.0	
GBAA3668	Glycosyl hydrolase, family 18				2.8	
GBAA3703	Phospholipase/carboxylesterase family protein				2.4	
GBAA3877	Hydrolase, alpha/beta fold family		2.0			
GBAA3878	Glyoxalase family protein	4.4	18.2	12.1	12.2	
GBAA4324	Hydrolase, alpha/beta fold family, putative			2.1		
GBAA4588	Glyoxalase family protein, authentic frameshift				2.6	
GBAA4593	Acetyltransferase, GNAT family				2.8	
Fatty acid and phospholipid metabolism						
GBAA2053	Cytosolic long-chain acyl-CoA thioester hydrolase family protein				2.4	
GBAA4874	3-Oxoacyl-(acyl carrier protein) reductase, putative			2.4	2.3	
Menaquinone and ubiquinone						
GBAA5111	*menD*; 2-succinyl-6-hydroxy-2,4-cyclohexadiene-1-carboxylic acid synthase/2-oxoglutarate decarboxylase					2.2
Protein fate						
GBAA1903	Peptidase, M23/M37 family					30.8
GBAA5687	*msrA-2*; peptide methionine sulfoxide reductase			2.1	2.1	
Purines, pyrimidines, nucleosides, and nucleotides						
GBAA1797	*pyrH*; uridylate kinase					2.4
GBAA5209	5′-nucleotidase family protein, truncation				2.3	
Regulatory functions/DNA interactions						
GBAA1468	Transcriptional regulator, putative				2.2	
GBAA2530	Transcriptional regulator, TetR family			2.2	2.1	
GBAA2543	Transcriptional regulator, TetR family			2.0		
GBAA3328	Transcriptional regulator, AraC family			13.8	14.3	
GBAA4433	Sugar-binding transcriptional regulator, LacI family			2.7		
GBAA4699	Transcriptional regulator, MarR family				3.8	
GBAA5331	DNA-binding response regulator				2.0	

Continued on facing page

TABLE 3—*Continued*

Gene no. (*B. anthracis* Ames Ancestor genome)	Gene name and/or putative function[b]	Fold change in expression for the following comparison:				
		Sterne with LB plus paraquat vs LB alone (control)[c]		Δ*sodA1* mutant with LB plus paraquat vs LB alone (control)[d]		Δ*sodA1* mutant vs Sterne, both with LB alone[e]
		100 μM paraquat	800 μM paraquat	100 μM paraquat	800 μM paraquat	
Regulatory functions/protein interactions						
GBAA0994	Response regulator			3.5	3.3	
Riboflavin, FMN, and FAD						
GBAA4331	*ribD*; riboflavin biosynthesis protein RibD				3.3	
GBAA4332	*ribE*; riboflavin synthase, alpha subunit				3.2	
GBAA4333	*ribBA*; 3,4-dihydroxy-2-butanone 4-phosphate synthase/GTP cyclohydrolase II				2.6	
Siderophore biosynthesis						
GBAA1981	Siderophore biosynthesis protein, putative				2.5	
GBAA2368	*entA*; 2,3-dihydro-2,3-dihydroxybenzoate dehydrogenase		7.3	64.7	76.7	
GBAA2369	*dhbC*; isochorismate synthase DhbC		10.0	134.8	163.5	
GBAA2370	*dhbE*; 2,3-dihydroxybenzoate-AMP ligase		9.1	74.2	86.8	
GBAA2371	*dhbB*; isochorismatase	5.6	12.8	76.7	88.1	
GBAA2372	*dhbF*; nonribosomal peptide synthetase DhbF	3.7	8.9	46.7	52.3	
GBAA2373[f]	*mbtH*-like protein	4.3	11.4	49.8	53.1	
GBAA2374[f]	Drug resistance transporter, EmrB/QacA family	4.2	11.0	64.4	76.8	
GBAA2375[f]	4′-phosphopantetheinyl transferase, putative		8.5	28.6	32.6	
Sporulation and germination						
GBAA0521	*yfhP* protein			2.3	2.0	
GBAA0767	*spoVR*; stage V sporulation protein R			2.7	2.9	
GBAA1979	*sapB* protein				2.0	
GBAA1987	Small, acid-soluble spore protein, alpha/beta family		2.5	4.1	2.9	
GBAA5528	*spoIID*; stage II sporulation protein D					3.3
Transcription factors						
GBAA2454	RNA polymerase sigma-70 factor, ECF subfamily		5.5			
Transport and binding proteins						
GBAA0228	ABC transporter, ATP-binding protein					2.0
GBAA0314	ABC transporter, substrate-binding protein, putative			3.6	2.9	
GBAA0349	Iron compound ABC transporter, permease protein			7.9	7.6	
GBAA0350	Iron compound ABC transporter, permease protein			6.2	6.3	
GBAA0351	Iron compound ABC transporter, iron compound-binding protein			3.8	4.3	
GBAA0378	Anaerobic C_4-dicarboxylate membrane transporter					2.5
GBAA0528	ABC transporter, ATP-binding/permease protein			2.3		
GBAA0532	ABC transporter, ATP-binding protein		2.1			
GBAA0534	ABC transporter, permease protein, putative		2.1			
GBAA0535	Potassium channel protein, putative		2.2			
GBAA0593	Amino acid permease family protein					2.0
GBAA0615	Iron compound ABC transporter, iron compound-binding protein					2.0
GBAA0616	Iron compound ABC transporter, permease protein				3.0	
GBAA0617	Iron compound ABC transporter, permease protein			2.2	2.7	
GBAA0618	Iron compound ABC transporter, ATP-binding protein			2.6	2.5	2.1
GBAA0739	*kdpA*; potassium-transporting ATPase, A subunit				2.8	

Continued on following page

TABLE 3—*Continued*

Gene no. (*B. anthracis* Ames Ancestor genome)	Gene name and/or putative function[b]	Fold change in expression for the following comparison:				
		Sterne with LB plus paraquat vs LB alone (control)[c]		Δ*sodA1* mutant with LB plus paraquat vs LB alone (control)[d]		Δ*sodA1* mutant vs Sterne, both with LB alone[e]
		100 μM paraquat	800 μM paraquat	100 μM paraquat	800 μM paraquat	
GBAA0740	*kdpB*; potassium-transporting ATPase, B subunit				2.5	
GBAA0741	*kdpC*; potassium-transporting ATPase, C subunit			2.1	2.4	
GBAA0787	Major facilitator family transporter		2.1		2.7	
GBAA1652	Permease, putative	39.8	147.6	69.8	75.7	
GBAA1825	Multidrug resistance protein, putative, authentic frameshift			2.5	2.3	
GBAA1858	Major facilitator family transporter			3.9	3.2	
GBAA1890	Homoserine/threonine efflux protein, putative			2.7		
GBAA2255	Substrate-binding family protein, putative			5.0	7.1	
GBAA2277	Permease, putative		6.2		2.2	
GBAA2279	*proV-1*; glycine betaine/L-proline ABC transporter, ATP-binding protein				2.3	
GBAA2346	Major facilitator family transporter	10.5	75.1	33.7	34.2	
GBAA3429	*gntP-2*; gluconate permease		2.2			
GBAA3531	Iron compound ABC transporter, iron compound-binding protein, putative			9.7	13.4	
GBAA3533	Iron compound ABC transporter, permease protein			19.1	26.6	
GBAA3534	Iron compound ABC transporter, permease protein			6.6	8.3	
GBAA3864	Iron compound ABC transporter, ATP-binding protein		3.0	8.7	10.4	
GBAA3865	Iron compound ABC transporter, permease protein		3.3	13.9	15.7	
GBAA3866	Iron compound ABC transporter, permease protein		4.6	17.5	19.8	2.0
GBAA3867	This region contains an authentic frameshift and is not the result of an iron compound ABC transporter, iron compound-binding protein	4.9	7.4	7.7	8.5	
GBAA4305	Xanthine/uracil permease family protein					2.0
GBAA4595	Iron compound ABC transporter, ATP-binding protein			31.7	49.2	
GBAA4596	Iron compound ABC transporter, permease protein			29.7	53.2	
GBAA4597	Iron compound ABC transporter, iron compound-binding protein			39.3	64.7	
GBAA4652	Substrate-binding family protein, putative				3.5	
GBAA4726	Transporter, EamA family			2.9		
GBAA4784	Iron compound ABC transporter, ATP-binding protein			15.3	26.2	
GBAA4785	Iron compound ABC transporter, permease protein			13.9	25.5	
GBAA4786	Iron compound ABC transporter, iron compound-binding protein			39.4	69.4	
GBAA5064	*feoB*; ferrous iron transport protein B				2.6	
GBAA5219	ABC transporter, substrate-binding protein, putative			5.0	2.9	
GBAA5220	ABC transporter, substrate-binding protein, putative			2.9		
GBAA5260	Major facilitator family transporter	6.5	13.8	7.1	7.8	
GBAA5327	Iron compound ABC transporter, ATP-binding protein			2.5	2.6	
GBAA5328	Iron compound ABC transporter, permease protein			2.1	2.3	
GBAA5329	Iron compound ABC transporter, permease protein			2.2	2.5	
GBAA5411	ABC transporter, ATP-binding/permease protein			3.8	4.4	

Continued on facing page

TABLE 3—*Continued*

Gene no. (*B. anthracis* Ames Ancestor genome)	Gene name and/or putative function[b]	Fold change in expression for the following comparison:				
		Sterne with LB plus paraquat vs LB alone (control)[c]		Δ*sodA1* mutant with LB plus paraquat vs LB alone (control)[d]		Δ*sodA1* mutant vs Sterne, both with LB alone[e]
		100 μM paraquat	800 μM paraquat	100 μM paraquat	800 μM paraquat	
GBAA5628	Iron compound ABC transporter, iron compound-binding protein					2.0
GBAA5629	Iron compound ABC transporter, ATP-binding protein			3.3	3.4	
GBAA5630	Iron compound ABC transporter, permease protein				5.5	
GBAA5631	Iron compound ABC transporter, permease protein, degenerate			6.0	6.9	
Unknown functions						
GBAA1454	PspA/IM30 family protein		4.6			
GBAA2016	Bacterial luciferase family protein		3.0	4.3	4.5	
GBAA3060	MutT/nudix family protein			2.4		
GBAA3876	Phosphoglycerate mutase family protein, putative		2.1			
GBAA4257	Class II aldolase/adducin domain protein			3.6		
GBAA4594	Ankyrin repeat domain protein		2.3	25.4	32.9	
GBAA4720	ThiJ/PfpI family protein			2.6	2.4	
GBAA4789	LPXTG-motif cell wall anchor domain protein, putative			72.4	118.9	
GBAA5065	FeoA family protein			2.3	3.4	

[a] As outlined in Fig. 1B. Also included are genes differentially expressed by the untreated Δ*sodA1* mutant versus the untreated parental strain, Sterne, both in LB only.
[b] MBR, membrane-localized benzodiazepine receptor; GNAT, GCN5-related *N*-acetyltransferase; CoA, coenzyme A; ECF, extracytoplasmic function.
[c] SAM comparison 1 in Fig. 1B.
[d] SAM comparison 2 in Fig. 1B.
[e] SAM comparison 3 in Fig. 1B.
[f] Included under "Siderophore biosynthesis" because of cotranscription, although not annotated as such in the TIGR Gene Ontology (GO) and TIGRFAM tables.

Δ*sodA1* mutant, whereas 113 are significantly underexpressed (Table 3, last column; see also the tables in the supplemental material). The low ratio of overexpressed versus underexpressed genes (0.22 in this comparison, versus 1.3 for Sterne and 2.4 for the Δ*sodA1* mutant in response to 800 μM paraquat) is notable because underexpression of genes cannot be explained merely by slower growth, since this mutant grows equivalently to Sterne in LB medium (Fig. 1A). Many of the genes underexpressed by the Δ*sodA1* mutant encode proteins with unknown biological functions, a common challenge encountered in many microarray experiments. Functional-family analysis (Table 2, last column) shows that even without induced superoxide stress, the Δ*sodA1* mutant expresses several transport and binding genes and metabolic genes at higher levels than Sterne, suggesting that this mutant is undergoing endogenous superoxide stress or an undefined oxidative stress simply as a result of normal metabolism, without the addition of a redox cycling compound, and that this stress does not result in a lower growth rate.

One prominent group of genes overexpressed by the Δ*sodA1* mutant during logarithmic growth consists of GBAA1778, -1779, and -1780 (up-regulated 49-, 23-, and 31-fold, respectively). An operon prediction algorithm developed by Bergman et al. (5) predicts that the first two genes are most certainly transcribed as one unit, whereas inclusion of the third gene is less certain. End point RT-PCR using primers designed to amplify overlapping gene regions showed that these three genes are, in fact, transcribed as one unit (data not shown). It can reasonably be assumed that the first two genes, a putative cytochrome *c*-type biogenesis protein (*ccdA-1*) and a putative thioredoxin family protein, are related to the general cellular redox status of the cell. Homologs of these two genes are located together on the genomes of diverse microorganisms such as *Streptococcus pyogenes*, *Clostridium tetani*, *Dehalococcoides ethenogenes*, and *Thermoanaerobacter tengcongensis* (genome region comparison performed at http://cmr.tigr.org). However, the third protein, a putative prolipoprotein diacylglyceryl transferase, is located just downstream of the other two only in the pathogenic *Bacillus cereus* group (*B. anthracis*, *B. cereus*, and *B. thuringiensis*) as far as the current TIGR database of sequenced genomes can reveal. The polycistronic nature of these proteins in the pathogenic *Bacillus cereus* group is unknown and may merit further investigation. This example highlights the way in which combining various bioinformatic approaches can reveal potentially interesting phenomena that may not be observed otherwise.

The remaining genes expressed at higher levels by the Δ*sodA1* mutant during normal growth encode a variety of proteins, including menaquinone (GBAA5111), uridylate kinase (*pyrH*; GBAA1797), a putative membrane protein (GBAA1904), acid phosphatase (GBAA4746), DNA topoisomerase III (*topB-2*; GBAA1905), various transporters, and others (Tables 2 and 3, last columns); most showed moderate increases in expression, ranging from two- to fourfold relative

to wild-type levels. The only other gene whose expression was notably increased to very high levels in the Δ*sodA1* mutant during normal growth encodes an M23/M37 family peptidase. It is reasonable to predict that the Δ*sodA1* mutant may harbor higher levels of protein damage from oxidative stress during aerobic growth than the parental strain. This topic is currently under investigation.

The relatively high expression levels of these genes in the Δ*sodA1* mutant compared to the parental strain without paraquat stress highlight the complex, multifactorial ways in which even minor changes in intracellular redox conditions (i.e., as a result of the lack of a major antioxidant enzyme) can affect gene regulation. The data below, on the other hand, showing differences in gene expression after treatment with different concentrations of paraquat, most likely reflect changes in gene regulation due to multiple downstream effects caused by an initial increase in intracellular superoxide levels imposed by paraquat. For example, because SODs themselves generate H_2O_2 during their enzymatic dismutation of superoxide, and since the Δ*sodA1* mutant lacks the most effective form of SOD, wild-type cells may potentially be responding to higher levels of H_2O_2. Superoxide itself can cause various effects (including protein damage, metal ion stability, accumulation of H_2O_2 due to the action of SOD proteins, impaired enzymatic functions of redox sensitive enzymes, etc.), and the various transcriptional differences seen in treated versus untreated cells most likely reflect various levels of shifts in homeostasis. Regardless of the exact mechanisms, the global changes reflect the ways in which *B. anthracis* has evolved to handle both major and minor shifts in intracellular redox conditions. The annotated genomes of *B. anthracis* strains have no homolog to the well-defined *E. coli soxR soxS* superoxide-sensitive regulatory system (65), and the various regulatory networks of *B. anthracis* have been only partially characterized (31).

Functional-family analysis and SAM comparing gene families and individual genes expressed differentially after exposure to paraquat. (i) Functional families. Functional-family analysis is a useful way to view the overall, end point character of an induced transcriptional response. Table 2 lists the families of genes that are significantly overrepresented within the subset of *B. anthracis* genes that change significantly after treatment with paraquat. The most evident trend is the large number of transport and binding protein genes and siderophore biosynthesis genes more highly expressed upon paraquat exposure, suggesting that oxidative stress is tightly correlated with metal ion homeostasis. It should be noted that very few transport proteins have been characterized in *B. anthracis* (33). However, it is clear that (i) a higher dose of paraquat induces the transcription of a greater number of putative transport proteins in Sterne, and (ii) at both doses, the Δ*sodA1* mutant expresses at least threefold more genes in this category than Sterne, once again suggesting that *sodA1* maintains intracellular redox conditions that affect gene transcription.

The transcriptional response of the Δ*sodA1* mutant to paraquat was exaggerated compared with that of the parental Sterne strain (Tables 2 and 3, compare Sterne to Δ*sodA1* columns). The Sterne strain responded to 100 μM paraquat by inducing the expression of 19 genes, with no genes underexpressed, while the Δ*sodA1* mutant increased the transcription of 119 genes twofold or more and decreased the transcription of 17 genes. The difference in the increase in transcription between these two strains (sixfold higher for the Δ*sodA1* mutant) highlights the importance of *sodA1* in maintaining levels of intracellular redox homeostasis that may result in the transcription of many genes. Addition of the higher concentration of paraquat (800 μM) resulted in a larger number of genes differentially expressed in Sterne (59 up-regulated; 45 down-regulated), while the Δ*sodA1* mutant again responded more strongly (154 up-regulated; 64 down-regulated). Note that the increased transcription in the Δ*sodA1* mutant in response to the low dose of paraquat was still substantially higher than that of Sterne in response to an eightfold-higher dose, once more stressing the importance of *sodA1* to intracellular redox maintenance. Also note that several genes were detected as more highly expressed in the Δ*sodA1* mutant at the lower dose of paraquat and not at the higher dose (Table 3, Δ*sodA1* columns). Unlike those of the Sterne strain, the growth kinetics of the Δ*sodA1* mutant are affected at this concentration of paraquat: upon addition of 800 μM paraquat to logarithmically growing cells, the rise in OD_{600} levels off and then begins to decrease after about 4 h of exposure, showing that this concentration of reagent eventually proves lethal to this mutant (62). Hence, it is not surprising that some unexpected trends may be observed at this dose with the mutant strain. The majority of genes induced in the Δ*sodA1* mutant, however, are detected after treatment with both doses of paraquat at levels well above twofold relative to the control, and many of these genes have very clear connections to redox functions [e.g., NAD(P)H dehydrogenase, flavodoxins, and nitroreductase family protein (Table 3)].

Curiously, none of the *B. anthracis sod* genes showed increased expression after 20 to 25 min of paraquat treatment. It is possible that a transient increase in expression may have occurred before RNA harvesting in these experiments. However, expression of the *sod* genes during logarithmic growth and entry into sporulation phase showed that three of the four *sod* genes are, for the most part, expressed constitutively (62). Ongoing studies also show that, in contrast to the pattern for *E. coli*, neither *sodA1* nor *sodA2* is expressed at higher levels in *B. anthracis* growing in iron-depleted medium than in rich medium (22, 23; also data not shown), and it is possible that *B. anthracis* has evolved less complex *sod* regulation than other bacteria. However, a study of *B. anthracis* gene expression during infection of macrophages identifies *sodA2* as showing increased expression during intracellular growth (N. H. Bergman et al., submitted for publication), an intriguing finding given that this isoform of the enzyme is not a major player in protection from oxidative stress and is not needed for survival in the susceptible mouse model (62).

(ii) Glyoxalase system. Notably, the expression of three separate putative glyoxalase family genes is greatly increased in both Sterne and the Δ*sodA1* mutant upon treatment with paraquat at both doses (increases of 37- to 85-fold for GBAA1653, 3- to 28-fold for GBAA3339, and 4- to 18-fold for GBAA3878 [Table 3]). The glyoxalase cycle is highly conserved in eukaryotes and prokaryotes, is important in certain types of cellular detoxification (16), and has been linked to potassium efflux in *E. coli* (51). The nucleophile methylglyoxal is a toxic but naturally occurring metabolite that can accumulate in cells as a result of various metabolic processes (9, 27), and the

glyoxalase system has evolved as a protective mechanism. The major protective glyoxalase system in *E. coli* is glutathione dependent (51), but it is believed that *B. anthracis* does not use glutathione in cellular redox reactions (25), so the glyoxalase system(s) in *B. anthracis* is presumably non-glutathione dependent. Note that the annotated *B. anthracis* Ames Ancestor genome lists 18 unique "glyoxalase family proteins" (6 of which are spelled "glyoxylase"), further highlighting the high degree of potential redundancy encoded on the genome, a phenomenon that has been observed for this bacterium before (37).

Protein sequence comparisons reveal that the three *B. anthracis* glyoxalase paralogs identified in this study are homologous mainly to other gram-positive microorganisms such as *Bacillus*, *Staphylococcus*, and *Oceanobacillus* species. The disparate locations of the three genes on the chromosome and the concomitant change in expression in response to paraquat suggest a conserved regulation of the genes that is sensitive to superoxide or to downstream effects caused by rises in superoxide levels. We therefore investigated the toxicity of the compound methylglyoxal to *B. anthracis* Sterne cells before and after paraquat treatment. We found that priming vegetatively growing Sterne cells with 800 μM paraquat for 45 min in LB medium causes the cells to be slightly more resistant to methylglyoxal in a disk diffusion assay than cells grown without paraquat. A preliminary experiment demonstrating this trend led us to repeat the experiment with two independent starter strains and a larger number of replicates. The average zone of inhibition of untreated Sterne cells was ~25.5 mm (standard deviation, ±0.9), whereas cells that had been grown in the presence of 800 μM paraquat had an average zone diameter of 22.1 mm (standard deviation, ±0.7) ($n = 20$ for each condition, paraquat treatment or no treatment; $P < 0.0001$ by an unpaired, two-tailed Student t test; zones were measured independently by two investigators). The MIC of methylglyoxal for logarithmically growing cells that are back-diluted to an OD_{600} of 0.01 is between 200 μM (strong growth) and 300 μM (no growth). The ability of the paraquat-primed cells to be slightly more resistant to methylglyoxal suggests that at least part of the glyoxalase system in *B. anthracis* responds to intracellular redox stress. A putative glyoxalase has been identified as potentially contributing to the physiology of the major pathogen *Mycobacterium tuberculosis* (40). Also, studies of *B. anthracis* gene expression during macrophage infection indicate an increase in the expression of two putative glyoxalases (Bergman et al., submitted), different from those identified in this study, further highlighting the potentially multifaceted roles for glyoxalases in bacterial metabolism and virulence.

(iii) Siderophore biosynthetic genes and putative transporters. Siderophores are small metabolites synthesized by bacteria to scavenge iron from the extracellular milieu during iron limitation, and iron metabolism has been correlated with the virulence of various pathogens (10, 77). The *B. anthracis* siderophore biosynthetic genes up-regulated in response to paraquat, with one exception, were in the operon containing homologs to the *B. subtilis* bacillibactin biosynthetic genes (the *dhb* operon; the *B. anthracis* operon is referred to below as the *bac* operon) (53). The five *B. anthracis* genes GBAA2368 to -2373 share 60 to 70% protein identity with the *B. subtilis* homologs. It has been shown that *B. anthracis* produces the bacillibactin metabolite at low levels (48), but the major siderophore that *B. anthracis* uses for survival under iron-limiting conditions is a second molecule called petrobactin, which is synthesized by genes included in the *asb* operon (13, 49, 79). Up-regulation of bacillibactin biosynthetic genes and of other genes under the transcriptional control of the iron-responsive regulator *fur* in response to oxidative stress has been seen in *B. subtilis* (58). The regulation of the homologous genes in *B. subtilis* by the iron-responsive Fur element has been studied extensively (2, 53, 58, 61). However, the four putative *fur* family and iron-dependent regulators in *B. anthracis* have not been characterized, so direct correlation between *fur* regulation and oxidative stress cannot be verified here. The canonical *fur* binding sequences upstream of the *bac* operon, however, are identical in *B. subtilis* and *B. anthracis*, whereas the binding sequence upstream of the *asb* (petrobactin biosynthetic) operon is not entirely conserved (data not shown). This finding and the fact that, in contrast to the results for the *bac* operon, transcription of only one of the *asb* genes was shown to be slightly increased after paraquat treatment strongly suggest that these two biosynthetic operons are not subject to identical transcriptional control, at least under superoxide stress.

The bacillibactin biosynthetic gene cluster in *B. subtilis* is composed of five adjacent genes termed *dhbACEBF* (2, 12, 53, 67). The homologs in *B. anthracis* maintain this gene order (GBAA2368 to -2372), but in *B. anthracis*, three downstream genes (GBAA2373, -2374, and -2375) that are not present in the *B. subtilis dhb* region are also overexpressed after paraquat treatment at levels roughly equivalent to those observed for GBAA2368 to -2372 (Table 3, siderophore biosynthesis). Homologs of these three genes are often found near nonribosomal peptide synthesis operons in other bacteria (73), and the operon prediction algorithm described by Bergman et al. (5) predicts that cotranscription of these three genes in *B. anthracis* is highly probable. End point RT-PCR probing for overlapping transcription products confirms that these genes are included in the *B. anthracis bac* transcriptional unit (data not shown), further highlighting differences between *B. subtilis* and *B. anthracis*. The three genes encode an MbtH-like protein, an EmrB/QacA family drug-resistance transporter, and a putative 4′-phosphopantetheinyl transferase. The MbtH-like protein has approximately 56% identity with the *M. tuberculosis* homolog by ClustalW alignment, and homologs of this protein are found near nonribosomal peptide synthetases (73) in other bacteria. Although this small protein (~70 amino acids) is part of the operon for the biosynthesis of the very important mycobactin siderophore of *M. tuberculosis*, its function has not been determined (17). The connection with bacillibactin implied by the cocistronic structure suggests that these genes have an alternative function that has not yet been ascertained, or that they, too, are involved in the biosynthesis of bacillibactin in a way that is not conserved or not transcriptionally coupled in *B. subtilis*.

The last section of Table 3 lists the many putative transport and binding proteins that show increased expression after paraquat stress, primarily in the Δ*sodA1* mutant. Of the putative transporters that showed increased expression in response to paraquat only in the Δ*sodA1* mutant, many are annotated as putative iron compound transporters, and some of these show very large increases (up to 69-fold) in expression. Because these transporters are currently uncharacterized, it is difficult

TABLE 4. SYBR green quantitative RT-PCR results for select genes identified as significantly increased in expression by SAM

Gene[a]	Fold change in gene expression[b] by SYBR green quantitative RT-PCR for the following strain(s) and condition[c]:		
	Sterne + PQ	Δ*sodA1* mutant + PQ	Δ*sodA1* mutant in LB vs Sterne in LB
entA-dhbC	+24	+34	+7
asbA	+4	+10	−2
Glyoxalase family	+58	+27	0
ccdA-1	NP[d]	NP	+49
Thioredoxin family	NP	NP	+79
Prolipoprotein	NP	NP	+11

[a] Gene-specific primers amplify the following regions: for *entA-dhbC*, the overlapping region across the first two genes of the *bac* operon, GBAA2368 and GBAA2369; for *asbA*, the second gene in the *asb* operon (petrobactin biosynthetic genes), GBAA1982; for the glyoxalase family protein, GBAA3339; for *ccdA-1*, the cytochrome *c*-type biogenesis protein gene GBAA1778; for the thioredoxin family protein, GBAA1779; and for the prolipoprotein diacylglyceryl transferase family protein, GBAA1780.

[b] Normalized against expression by the *fusA* constitutive control. C_T values for *fusA* had a standard deviation of <1 cycle for all RNA samples (see Materials and Methods), ranging from 12.19 to 12.83.

[c] PQ, paraquat (800 μM).

[d] NP, not performed. These genes were not quantified by SYBR green quantitative RT-PCR for paraquat-treated samples.

to know whether they are specific for iron and whether they are responsible for metal influx or efflux. Regardless, the large number of genes with a putative iron transport role suggests a very large shift in iron homeostasis in the Δ*sodA1* mutant in response to paraquat (see "Growth of multiple *B. anthracis* Δ*sod* mutants in various metal-limiting media" below). Three general permease/major facilitator family transporter genes showed substantially increased expression in both Sterne and the Δ*sodA1* mutant after both paraquat treatments (39- to 147-fold for GBAA1652, 10- to 75-fold for GBAA2346, and 6- to 13-fold for GBAA5260 [Table 3]), suggesting that the expression of these genes is highly sensitive to intracellular superoxide levels or is somehow caused by the damage resulting from a rise in superoxide levels.

To confirm the increase in the expression of select genes that we observed with the microarrays, we performed SYBR green quantitative RT-PCR on a small subset of genes with fresh RNA samples (Table 4). As in the microarray experiments, a region within the *bac* operon was seen to be induced substantially after treatment with paraquat, whereas the expression of a gene from the *asb* operon was increased only slightly in Sterne and more in the Δ*sodA1* mutant. Additionally, the glyoxalase family gene GBAA3339 was seen to undergo a major increase in expression in response to paraquat. Lastly, the *ccdA-1* operon transcript was assayed from strains growing in LB alone, and the Δ*sodA1* mutant transcribed these genes at substantially higher levels than the parental Sterne strain during normal exponential growth. It should be noted that *n*-fold changes are not expected to be identical for the SYBR green assays and the microarrays, since normalization in the microarrays is extremely stringent, detecting 18 separate probes for each open reading frame, making for a much more robust system than the use of a single primer pair per gene as in the RT-PCR.

Isolation and quantification of the siderophores bacillibactin and petrobactin from *B. anthracis* grown in iron-depleted medium with and without paraquat stress. The striking increase in the transcription of the *bac* operon after paraquat stress led us to explore the possibility that the bacillibactin siderophore might be produced at higher levels after superoxide stress. *B. subtilis* is unable to grow in certain iron-poor media when it is unable to produce bacillibactin (61). In contrast, *B. anthracis* relies on petrobactin production for growth in iron-poor media (13), while Δ*bac* mutants grow as well as the wild type during iron limitation (13; also data not shown). Table 3 shows that the induction of the *bac* genes in response to paraquat was substantial in Sterne (ranging from 5- to 12-fold) and even more prominent in the Δ*sodA1* mutant (ranging from 42- to 163-fold). Of the *asb* biosynthetic genes, only one was more than twofold induced in response to 800 μM paraquat in the Δ*sodA1* mutant.

Koppisch et al. (48) report that petrobactin is the main siderophore produced in iron-limiting medium, with relatively low levels of bacillibactin produced. However, they observed that cultures grown in ambient air seemed to produce higher levels of bacillibactin. Quantities of intra- and extracellular bacillibactin and petrobactin from *B. anthracis* were monitored using LC-MS by isolating supernatants and lysates of exponentially growing cells of the Sterne, Δ*sodA1*, and Δ*bac* strains in iron-rich medium (LB) and IDM, with or without the addition of paraquat (Table 5). We note that siderophores are intricate metabolites, and the biosynthesis of these molecules is highly complex, involving the cooperation of a number of specific enzymes and cofactors to assemble them; hence, considering the complexity of these systems, expression of the biosynthetic proteins, construction of macromolecular complexes, and the appearance of the metabolite could be temporally distinct rather than coincident (for an overview of the siderophore "assembly line," see reference 17). Therefore, we isolated cell supernatants and lysates 1 h after paraquat treatment to allow time for protein translation and metabolite synthesis to occur. The LC-MS analysis revealed that neither bacillibactin nor petrobactin accumulated in supernatants or lysates of cells grown in iron-rich LB medium, with or without paraquat (data not shown). Intracellular bacillibactin accumulated in Sterne and the Δ*sodA1* mutant grown in IDM but was not detected in Δ*sodA1* lysates after paraquat treatment and was just barely detected in lysates of Sterne grown in the presence of paraquat. However, bacillibactin was detected in supernatants of Sterne and the Δ*sodA1* mutant grown in IDM, both with and without paraquat, but counter to what the transcriptional data suggest, the levels of bacillibactin were substantially decreased in paraquat-treated cells. A Δ*bac* mutant served as a negative control, and no bacillibactin was detected in this strain under any conditions. These data suggest that the expression of the *bac* genes in response to oxidative stress may be subject to additional layers of regulation (posttranscriptional) or that the added intracellular oxidative stress caused by paraquat may prevent various redox-sensitive enzymatic processes from occurring during the complex, multistep production of bacillibactin (17, 53). The Δ*bac* mutant shows sensitivities to paraquat and H_2O_2 identical to those of the parental Sterne $34F_2$ strain (data not shown), and thus bacillibactin does not appear to be playing an overt role in protection from oxidative stress. However, the conservation of a functional bacillibactin biosynthetic pathway may indicate an alternative role for bacillibactin in *B.*

TABLE 5. Quantification of the siderophores bacillibactin and petrobactin produced by *Bacillus anthracis* Sterne $34F_2$ and the Δ*sodA1* and Δ*bac* mutants grown in IDM[a] and harvested during exponential phase with or without paraquat addition

Strain and condition[b]	Intracellular or extracellular concn[c] of the following siderophore in IDM:			
	Bacillibactin		Petrobactin	
	Intracellular	Extracellular	Intracellular	Extracellular
Sterne $34F_2$ (parental)				
Without PQ	0.102 ± 0.052	0.849 ± 0.102	NO[d]	91.471 ± 10.581
With PQ	0.002 ± 0.001	0.118 ± 0.076	NO	41.570 ± 6.578
Δ*sodA1* mutant				
Without PQ	0.054 ± 0.007	1.181 ± 0.364	NO	98.495 ± 13.111
With PQ	NO	0.087 ± 0.024[e]	NO	11.638 ± 3.125[e]
Δ*bac* mutant				
Without PQ	NO	NO	NO	48.577 ± 8.601
With PQ	NO	NO	NO	23.427 ± 6.411

[a] Made as described previously (13, 49). Siderophore quantification was also performed in iron-rich (LB) medium with the same strains and under the same conditions as those listed in the table, but no siderophores were isolated in those experiments.

[b] Paraquat (PQ) concentration and incubation times before harvesting of cell lysates and supernatants for siderophore quantification are as follows: for exponentially growing cells, 800 μM paraquat was added at an OD_{600} of 0.4 to 0.5, and cells were harvested after 1 h.

[c] Intracellular concentrations are expressed as μg/mg of protein; extracellular concentrations are expressed as μg/ml of supernatant.

[d] NO, not observed.

[e] Of all the samples, the growth of the Δ*sodA1* mutant was slowed by the addition of paraquat, so the final OD_{600} of this sample was slightly lower than those of all others.

anthracis physiology that has not yet been observed, or it may indicate that bacillibactin has a mildly redundant but minor role in iron acquisition compared to petrobactin. Recently, it was shown that certain proteins of host cells are able to scavenge and bind bacillibactin but are less efficient at sequestering petrobactin, highlighting the role of the petrobactin biosynthetic cluster in the evolution of virulence (1).

Despite the lack of changes in expression of the *asb* operon in response to oxidative stress, the many putative iron transporters that showed increased expression during superoxide stress led us to assay the levels of the petrobactin siderophore in the Sterne, Δ*sodA1*, and Δ*bac* strains as well. Substantial levels of petrobactin were isolated from IDM culture supernatants of all strains, with or without paraquat, and as with bacillibactin, levels of petrobactin were decreased after paraquat treatment, again suggesting that enzyme function during siderophore production may be compromised by intracellular redox stress. But petrobactin was never detected in cell lysates

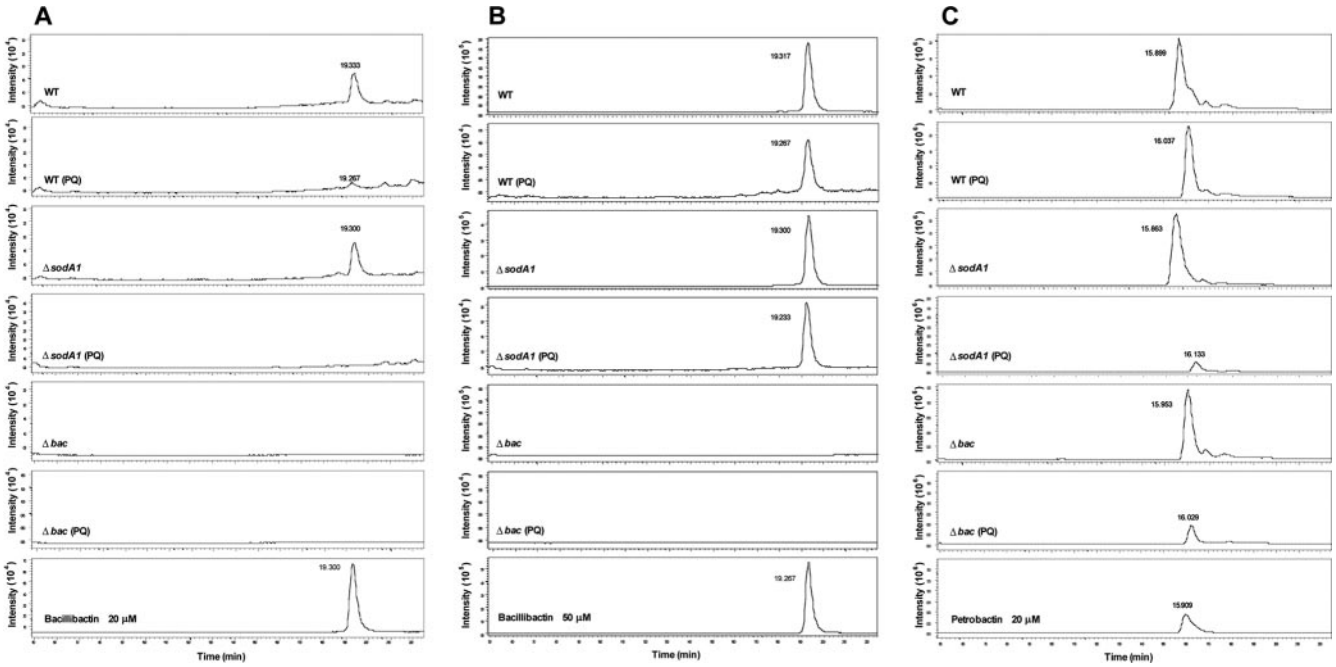

FIG. 2. LC-MS traces of extracts from the IDM culture supernatants and cell lysates of *B. anthracis* Sterne and the Δ*sodA1* and Δ*bac* mutants, showing the presence of bacillibactin or petrobactin. (A and B) SIM chromatograms of intracellular (A) and extracellular (B) bacillibactin at the mass range of *m/z* 883.2 $[M+H]^+$. Peaks at 19.230 to 19.340 min represent bacillibactin. (C) SIM chromatogram of extracellular petrobactin at the mass range of *m/z* 719.3 $[M+H]^+$. Peaks at 15.860 to 16.134 min represent petrobactin. PQ, paraquat-treated medium.

(Table 5; Fig. 2), suggesting that petrobactin synthesis and export may be tightly coupled. The study of siderophore transport has focused mainly on the process of metal import (11, 26, 55), while the process of siderophore export has been studied less extensively, and primarily for the gram-negative organism *E. coli* (7, 32). A spatial study of siderophore biosynthesis and export would be of great interest. It should be noted that bacillibactin and petrobactin were also quantified by HPLC from cells grown to stationary phase for 24 h (data not shown) and that these data showed the same trend of decreased siderophore concentrations after paraquat treatment.

Growth of multiple *B. anthracis* Δ*sod* mutants in various metal-limiting media. Iron homeostasis and oxidative stress are often linked biologically (60, 71, 72, 78), and the increased expression of the bacillibactin biosynthetic operon and numerous putative, uncharacterized transporters after paraquat stress that we observed was suggestive of an iron starvation response, especially for the Δ*sodA1* mutant. Although high intracellular iron levels in the cytoplasm can be toxic, especially in the presence of reactive oxygen, where they can lead to the formation of very damaging hydroxyl radicals (41), evidence from *E. coli* suggests that a lack of SOD can, counter to intuition, lead to an iron starvation phenotype, even in the presence of ample cytoplasmic iron (52). Maringanti and Imlay propose that in the presence of superoxide, *E. coli sod* mutants acquire damage to various iron-containing proteins, leading to the release of free iron that is "not usable," causing the bacteria to import new, "usable" iron for the repair of damaged enzymes, all the while accumulating potentially toxic levels of "unusable" intracellular free iron (52). With this precedent in mind, we tested the growth of several *B. anthracis* Δ*sod* mutants in a variety of iron/cation-limiting media to determine if these mutants have a higher need for iron/cation transport. This question is of particular interest due to the fact that the host environment is believed to be both iron limiting and potentially oxidatively challenging.

We tested bacterial growth in two different types of iron-limiting media: chelated and depleted. Chelated medium has the cation chelator (in this case, 2,2′-dipyridyl) present at all times, in effect binding metal and preventing its uptake in a concentration-dependent manner, whereas depleted medium has had the majority, but not the entirety, of metal salts preremoved with a resin (Bio-Rad Chelex 100) and has then been supplemented with several metal salts (e.g., magnesium and/or manganese). Consequently, chelated medium can effectively shut or slow down transport by holding ions unavailable, whereas depleted medium (IDM or IMnDM) allows ample transport, but with smaller amounts of various ions present for utilization.

Figure 3 depicts growth curves of multiple *B. anthracis* strains in LB medium containing either no chelating agent or the metal-chelating compound 2,2′-dipyridyl at 300 or 400 μM. The Δ*asb* mutant strain, which does not produce the siderophore petrobactin (79) and has been shown to have a growth defect in iron-poor medium (13, 49), was included as an indicator of iron depletion. Also included in these experiments were the Δ*sodA2* strain, lacking the second active *B. anthracis* SOD, and the Δ*sodA1* Δ*sodA2* strain, lacking both active SODs.

At both concentrations of 2,2′-dipyridyl, the Δ*asb* strain is most affected, confirming the importance of the siderophore petrobactin for *B. anthracis* under extremely iron poor conditions. The parental strain, Sterne, and the Δ*sodA2* mutant grow identically and to a lower final OD_{600} in the presence of 2,2′-dipyridyl. As with *E. coli* (52), the *B. anthracis* Δ*sodA1* mutant and the Δ*sodA1* Δ*sodA2* double mutant show a consistent growth defect in chelated medium, supporting the idea that only *sodA1* is needed for optimal physiological superoxide homeostasis during iron limitation and that no redundancy exists between *sodA1* and *sodA2* (62). Additionally, the MICs of

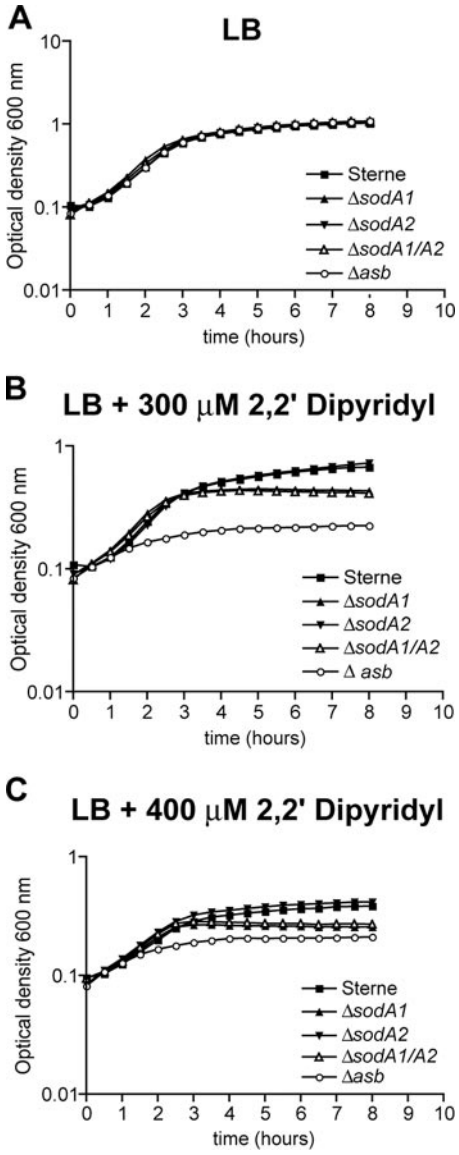

FIG. 3. Growth of *B. anthracis* Sterne ($34F_2$), the Δ*sodA1*, Δ*sodA2*, and Δ*asb* mutants, and the Δ*sodA1* Δ*sodA2* double mutant in untreated rich (LB) broth (A) and in the same medium chelated with 300 μM (B) or 400 μM (C) 2,2′-dipyridyl. The Δ*asb* mutant displayed the most severe growth defect in chelated medium, while the Δ*sodA1* mutant and Δ*sodA1* Δ*sodA2* double mutant showed consistent attenuation at both 2,2′-dipyridyl concentrations. The Δ*bac* strain displayed growth identical to that of the Sterne parental strain (data not shown). Results from one experiment representative of three independent experiments displaying the same trend are shown.

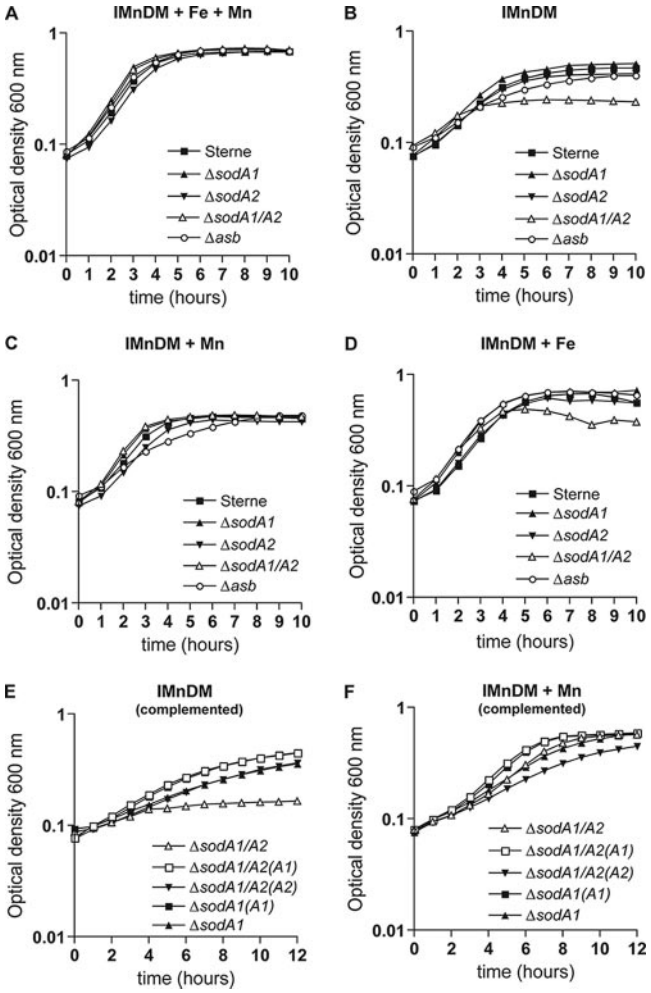

FIG. 4. Growth of *B. anthracis* Δ*sod* and Δ*asb* mutants and *sod*-complemented strains in metal-depleted media. Mn, 20 μM $MnSO_4 \cdot H_2O$; Fe, 20 μM $Fe(II)SO_4 \cdot 7H_2O$. (A to D) Growth of Sterne and the Δ*sod* and Δ*asb* mutants over time under the conditions indicated. (E and F) Growth of complemented strains over time. (A1) and (A2) indicate the presence of the wild-type *sodA1* and *sodA2* genes, respectively, on a cytoplasmic plasmid. The Δ*bac* strain displayed growth identical to that of the Sterne parental strain under all conditions (data not shown). Results from one experiment representative of three independent experiments displaying the same trends are shown.

2,2′-dipyridyl that prevent the outgrowth of spores of the Δ*sodA1* and Δ*sodA1* Δ*sodA2* mutants are between 200 and 300 μM, whereas the MICs for spores of Sterne and the Δ*sodA2* mutant are above 500 μM, with outgrowth sometimes occurring for these strains above 500 μM (data not shown).

Because 2,2′-dipyridyl binds multiple cations in a complex manner, we chose to further explore the growth of the Δ*sod* mutants in two different depleted media, where low concentrations of metal ions are available for transport and the presence of specific metal ions can be manipulated. IMnDM was prepared as described in Materials and Methods and previously (13). When ferrous iron (Fe) and manganese (Mn) were added back into IMnDM, all strains grew equivalently (Fig. 4A). Surprisingly, in IMnDM with no Fe or Mn supplementation, only the Δ*sodA1* Δ*sodA2* double mutant showed a severe growth defect, while even the Δ*asb* mutant showed only mild attenuation. The ability of the Δ*asb* mutant to eventually "catch up" to Sterne in IMnDM, compared to its severe growth defect in chelated medium, suggested that iron is still somewhat present and available even after resin depletion. Mn supplementation alone caused total recovery for the Δ*sodA1* Δ*sodA2* double mutant but not for the Δ*asb* mutant (Fig. 4C), while Fe supplementation alone allowed recovery only for the Δ*asb* mutant (Fig. 4D), confirming that these two phenotypes are Mn and Fe specific, respectively. Growth in IMnDM of complementation strains of the Δ*sodA1* Δ*sodA2* double mutant, expressing the wild-type *sodA1* or *sodA2* gene on a cytoplasmic plasmid (Fig. 4E and F), showed that (i) the presence of *sodA1* is necessary for the most robust growth during Mn limitation; (ii) the presence of *sodA2* allows for a slightly lower level of recovery; and (iii) the absence of both enzymes causes a severe growth defect in low-Mn medium. The Δ*sodA1* Δ*sodA2* double mutant is identical to the Δ*sodA1* single mutant in terms of sensitivity to paraquat and diamide (data not shown), and these results represent the first instance where the two mutants have exhibited differing behavior and suggest a mild redundancy for *sodA1* and *sodA2*. The *sodA2* gene is actively transcribed and encodes an active SOD enzyme (62), so a level of redundancy would be expected between these two enzymes. These data, however, still support the preeminence of *sodA1* as the more effective and/or more utilized of the two enzymes. Since iron is only slightly limiting in IMnDM, the possibility exists that one or both of the SODs might be cambialistic (able to utilize Mn or Fe as a catalytic ion). Regardless, as with *E. coli*, the *B. anthracis* Δ*sodA1* and Δ*sodA1* Δ*sodA2* mutants behaved as if they were iron starved, and the presence of various intracellular iron pools under oxidative stress is currently being investigated.

Summary and conclusions. In this study, we used Affymetrix DNA microarrays to examine the global transcriptional responses of the *B. anthracis* wild-type Sterne and Δ*sodA1* mutant strains to different levels of intracellular superoxide stress generated endogenously by the compound paraquat. This global approach identified various groups of genes that showed increased transcription after different levels of oxidative stress in two strains that are differentially sensitive to paraquat. First, a small set of genes showed increased transcription in the Δ*sodA1* mutant relative to the parental strain during normal growth in rich broth, independently of induced chemical stress. Because most of these genes were not induced in the parental strain after paraquat stress, their regulation may be controlled by an as yet unidentified, paraquat-independent effect that a lack of *sodA1* may facilitate. Next, a group of genes showed increased expression in Sterne in response to a low concentration of paraquat (100 μM); all these genes showed even higher induction in Sterne after exposure to 800 μM paraquat, and all of them were induced under both conditions in the Δ*sodA1* mutant. We propose that these genes may be under the control of a regulatory system that is quite sensitive to the presence of superoxide or to the damage caused by this reactive metabolite. Still other genes were induced only at the higher concentration of paraquat in Sterne and at both concentrations in the Δ*sodA1* mutant, likely representing a level of regulation less sensitive to superoxide stress than that for the previous group. Lastly, we observed an increase in the transcription of many

genes only in the Δ*sodA1* mutant at both concentrations of paraquat; these genes may be under the control of regulatory systems that respond only to very high levels of superoxide or oxidative damage that can be metabolically controlled when *sodA1* is present. The data presented here highlight the intrinsic and often contradictory connection between oxidative stress and metal acquisition in bacteria and indicate that *B. anthracis* has evolved multiple mechanisms to cope with these problematic conditions, which may be encountered within the host. We hope that the trends elucidated here will aid in the further investigation of the metabolic and regulatory processes used by the important pathogen *B. anthracis*.

ACKNOWLEDGMENTS

Special thanks go to the University of Michigan Affymetrix cDNA Core. Additional thanks go to Brian Janes, Aimee Richard, the David Sherman lab, and Stephen Cendrowski.

Funding for this work was provided by the University of Michigan Cellular Biotechnology Training Program, the University of Michigan F. G. Novy Fellowship, HHS contract N266200400059C/N01-A1-40059, NIH grant AI08649, and the Great Lakes Center of Excellence for Biodefense and Emerging Infections.

REFERENCES

1. **Abergel, R. J., M. K. Wilson, J. E. Arceneaux, T. M. Hoette, R. K. Strong, B. R. Byers, and K. N. Raymond.** 2006. Anthrax pathogen evades the mammalian immune system through stealth siderophore production. Proc. Natl. Acad. Sci. USA **103:**18499–18503.
2. **Baichoo, N., T. Wang, R. Ye, and J. D. Helmann.** 2002. Global analysis of the *Bacillus subtilis Fur* regulon and the iron starvation stimulon. Mol. Microbiol. **45:**1613–1629.
3. **Balboa, M. A., and J. Balsinde.** 2006. Oxidative stress and arachidonic acid mobilization. Biochim. Biophys. Acta **1761:**385–391.
4. **Bergman, N. H., E. C. Anderson, E. E. Swenson, M. M. Niemeyer, A. D. Miyoshi, and P. C. Hanna.** 2006. Transcriptional profiling of the *Bacillus anthracis* life cycle in vitro and an implied model for regulation of spore formation. J. Bacteriol. **188:**6092–6100.
5. **Bergman, N. H., K. D. Passalacqua, P. C. Hanna, and Z. S. Qin.** 2007. Operon prediction in sequenced bacterial genomes without experimental information. Appl. Environ. Microbiol. **73:**846–854.
6. **Bernhardt, J., J. Weibezahn, C. Scharf, and M. Hecker.** 2003. *Bacillus subtilis* during feast and famine: visualization of the overall regulation of protein synthesis during glucose starvation by proteome analysis. Genome Res. **13:** 224–237.
7. **Bleuel, C., C. Grosse, N. Taudte, J. Scherer, D. Wesenberg, G. J. Krauss, D. H. Nies, and G. Grass.** 2005. TolC is involved in enterobactin efflux across the outer membrane of *Escherichia coli*. J. Bacteriol. **187:**6701–6707.
8. **Bolstad, B. M., R. A. Irizarry, M. Astrand, and T. P. Speed.** 2003. A comparison of normalization methods for high density oligonucleotide array data based on variance and bias. Bioinformatics **19:**185–193.
9. **Booth, I. R., G. P. Ferguson, S. Miller, C. Li, B. Gunasekera, and S. Kinghorn.** 2003. Bacterial production of methylglyoxal: a survival strategy or death by misadventure? Biochem. Soc. Trans. **31:**1406–1408.
10. **Braun, V.** 2005. Bacterial iron transport related to virulence. Contrib. Microbiol. **12:**210–233.
11. **Brown, J. S., and D. W. Holden.** 2002. Iron acquisition by Gram-positive bacterial pathogens. Microbes Infect. **4:**1149–1156.
12. **Bsat, N., and J. D. Helmann.** 1999. Interaction of *Bacillus subtilis* Fur (ferric uptake repressor) with the *dhb* operator in vitro and in vivo. J. Bacteriol. **181:**4299–4307.
13. **Cendrowski, S., W. MacArthur, and P. Hanna.** 2004. *Bacillus anthracis* requires siderophore biosynthesis for growth in macrophages and mouse virulence. Mol. Microbiol. **51:**407–417.
14. **Chang, W., D. A. Small, F. Toghrol, and W. E. Bentley.** 2006. Global transcriptome analysis of *Staphylococcus aureus* response to hydrogen peroxide. J. Bacteriol. **188:**1648–1659.
15. **Chang, W., D. A. Small, F. Toghrol, and W. E. Bentley.** 2005. Microarray analysis of *Pseudomonas aeruginosa* reveals induction of pyocin genes in response to hydrogen peroxide. BMC Genomics **6:**115.
16. **Cordell, P. A., T. S. Futers, P. J. Grant, and R. J. Pease.** 2004. The human hydroxyacylglutathione hydrolase (HAGH) gene encodes both cytosolic and mitochondrial forms of glyoxalase II. J. Biol. Chem. **279:**28653–28661.
17. **Crosa, J. H., and C. T. Walsh.** 2002. Genetics and assembly line enzymology of siderophore biosynthesis in bacteria. Microbiol. Mol. Biol Rev. **66:**223–249.
18. **Culotta, V. C., M. Yang, and T. V. O'Halloran.** 2006. Activation of superoxide dismutases: putting the metal to the pedal. Biochim. Biophys. Acta **1763:**747–758.
19. **Dahlgren, C., and A. Karlsson.** 1999. Respiratory burst in human neutrophils. J. Immunol. Methods **232:**3–14.
20. **Dalle-Donne, I., R. Rossi, R. Colombo, D. Giustarini, and A. Milzani.** 2006. Biomarkers of oxidative damage in human disease. Clin. Chem. **52:**601–623.
21. **Dixon, T. C., M. Meselson, J. Guillemin, and P. C. Hanna.** 1999. Anthrax. N. Engl. J. Med. **341:**815–826.
22. **Dubrac, S., and D. Touati.** 2000. Fur positive regulation of iron superoxide dismutase in *Escherichia coli*: functional analysis of the *sodB* promoter. J. Bacteriol. **182:**3802–3808.
23. **Dubrac, S., and D. Touati.** 2002. Fur-mediated transcriptional and post-transcriptional regulation of FeSOD expression in *Escherichia coli*. Microbiology **148:**147–156.
24. **Eberhardt, M. K.** 2001. Reactive oxygen metabolites: chemistry and medical consequences. CRC Press, Boca Raton, FL.
25. **Fahey, R. C., W. C. Brown, W. B. Adams, and M. B. Worsham.** 1978. Occurrence of glutathione in bacteria. J. Bacteriol. **133:**1126–1129.
26. **Ferguson, A. D., and J. Deisenhofer.** 2004. Metal import through microbial membranes. Cell **116:**15–24.
27. **Ferguson, G. P., S. Totemeyer, M. J. MacLean, and I. R. Booth.** 1998. Methylglyoxal production in bacteria: suicide or survival? Arch. Microbiol. **170:**209–218.
28. **Forman, H. J., and M. Torres.** 2002. Reactive oxygen species and cell signaling: respiratory burst in macrophage signaling. Am. J. Respir. Crit. Care Med. **166:**S4–S8.
29. **Forman, H. J., and M. Torres.** 2001. Redox signaling in macrophages. Mol. Aspects Med. **22:**189–216.
30. **Foster, P. L.** 2005. Stress responses and genetic variation in bacteria. Mutat. Res. **569:**3–11.
31. **Fouet, A., and M. Mock.** 2006. Regulatory networks for virulence and persistence of *Bacillus anthracis*. Curr. Opin. Microbiol. **9:**160–166.
32. **Furrer, J. L., D. N. Sanders, I. G. Hook-Barnard, and M. A. McIntosh.** 2002. Export of the siderophore enterobactin in *Escherichia coli*: involvement of a 43 kDa membrane exporter. Mol. Microbiol. **44:**1225–1234.
33. **Gat, O., I. Mendelson, T. Chitlaru, N. Ariel, Z. Altboum, H. Levy, S. Weiss, H. Grosfeld, S. Cohen, and A. Shafferman.** 2005. The solute-binding component of a putative Mn(II) ABC transporter (MntA) is a novel *Bacillus anthracis* virulence determinant. Mol. Microbiol. **58:**533–551.
34. **Gobert, A. P., S. Semballa, S. Daulouede, S. Lesthelle, M. Taxile, B. Veyret, and P. Vincendeau.** 1998. Murine macrophages use oxygen- and nitric oxide-dependent mechanisms to synthesize *S*-nitroso-albumin and to kill extracellular trypanosomes. Infect. Immun. **66:**4068–4072.
35. **Hampton, M. B., A. J. Kettle, and C. C. Winterbourn.** 1998. Inside the neutrophil phagosome: oxidants, myeloperoxidase, and bacterial killing. Blood **92:**3007–3017.
36. **Hecker, M., and U. Volker.** 2001. General stress response of *Bacillus subtilis* and other bacteria. Adv. Microb. Physiol. **44:**35–91.
37. **Heffernan, B. J., B. Thomason, A. Herring-Palmer, L. Shaughnessy, R. McDonald, N. Fisher, G. B. Huffnagle, and P. Hanna.** 2006. *Bacillus anthracis* phospholipases C facilitate macrophage-associated growth and contribute to virulence in a murine model of inhalation anthrax. Infect. Immun. **74:** 3756–3764.
38. **Helmann, J. D., M. F. Wu, A. Gaballa, P. A. Kobel, M. M. Morshedi, P. Fawcett, and C. Paddon.** 2003. The global transcriptional response of *Bacillus subtilis* to peroxide stress is coordinated by three transcription factors. J. Bacteriol. **185:**243–253.
39. **Hosack, D. A., G. Dennis, Jr., B. T. Sherman, H. C. Lane, and R. A. Lempicki.** 2003. Identifying biological themes within lists of genes with EASE. Genome Biol. **4:**R70.
40. **Huard, R. C., S. Chitale, M. Leung, L. C. Lazzarini, H. Zhu, E. Shashkina, S. Laal, M. B. Conde, A. L. Kritski, J. T. Belisle, B. N. Kreiswirth, J. R. Lapa e Silva, and J. L. Ho.** 2003. The *Mycobacterium tuberculosis* complex-restricted gene cfp32 encodes an expressed protein that is detectable in tuberculosis patients and is positively correlated with pulmonary interleukin-10. Infect. Immun. **71:**6871–6883.
41. **Imlay, J. A.** 2006. Iron-sulphur clusters and the problem with oxygen. Mol. Microbiol. **59:**1073–1082.
42. **Imlay, J. A.** 2003. Pathways of oxidative damage. Annu. Rev. Microbiol. **57:**395–418.
43. **Irizarry, R. A., B. M. Bolstad, F. Collin, L. M. Cope, B. Hobbs, and T. P. Speed.** 2003. Summaries of Affymetrix GeneChip probe level data. Nucleic Acids Res. **31:**e15.
44. **Irizarry, R. A., B. Hobbs, F. Collin, Y. D. Beazer-Barclay, K. J. Antonellis, U. Scherf, and T. P. Speed.** 2003. Exploration, normalization, and summaries of high density oligonucleotide array probe level data. Biostatistics **4:**249–264.
45. **Janes, B. K., and S. Stibitz.** 2006. Routine markerless gene replacement in *Bacillus anthracis*. Infect. Immun. **74:**1949–1953.
46. **Johnson, F., and C. Giulivi.** 2005. Superoxide dismutases and their impact upon human health. Mol. Aspects Med. **26:**340–352.
47. **Katsuragi, H., M. Ohtake, I. Kurasawa, and K. Saito.** 2003. Intracellular

production and extracellular release of oxygen radicals by PMNs and oxidative stress on PMNs during phagocytosis of periodontopathic bacteria. Odontology **91:**13–18.
48. **Koppisch, A. T., C. C. Browder, A. L. Moe, J. T. Shelley, B. A. Kinkel, L. E. Hersman, S. Iyer, and C. E. Ruggiero.** 2005. Petrobactin is the primary siderophore synthesized by *Bacillus anthracis* str. Sterne under conditions of iron starvation. Biometals **18:**577–585.
49. **Lee, J. Y., B. K. Janes, K. D. Passalacqua, B. Pfleger, N. H. Bergman, H. Liu, K. Hakansson, R. V. Somu, C. C. Aldrich, S. Cendrowski, P. C. Hanna, and D. H. Sherman.** 2007. Biosynthetic analysis of the petrobactin siderophore pathway from *Bacillus anthracis*. J. Bacteriol. **189:**1698–1710.
50. **Li, H., A. K. Singh, L. M. McIntyre, and L. A. Sherman.** 2004. Differential gene expression in response to hydrogen peroxide and the putative PerR regulon of *Synechocystis* sp. strain PCC 6803. J. Bacteriol. **186:**3331–3345.
51. **MacLean, M. J., L. S. Ness, G. P. Ferguson, and I. R. Booth.** 1998. The role of glyoxalase I in the detoxification of methylglyoxal and in the activation of the KefB K^+ efflux system in *Escherichia coli*. Mol. Microbiol. **27:**563–571.
52. **Maringanti, S., and J. A. Imlay.** 1999. An intracellular iron chelator pleiotropically suppresses enzymatic and growth defects of superoxide dismutase-deficient *Escherichia coli*. J. Bacteriol. **181:**3792–3802.
53. **May, J. J., T. M. Wendrich, and M. A. Marahiel.** 2001. The *dhb* operon of *Bacillus subtilis* encodes the biosynthetic template for the catecholic siderophore 2,3-dihydroxybenzoate-glycine-threonine trimeric ester bacillibactin. J. Biol. Chem. **276:**7209–7217.
54. **Medini, D., C. Donati, H. Tettelin, V. Masignani, and R. Rappuoli.** 2005. The microbial pan-genome. Curr. Opin. Genet. Dev. **15:**589–594.
55. **Miethke, M., O. Klotz, U. Linne, J. J. May, C. L. Beckering, and M. A. Marahiel.** 2006. Ferri-bacillibactin uptake and hydrolysis in *Bacillus subtilis*. Mol. Microbiol. **61:**1413–1427.
56. **Moat, A. G., J. W. Foster, and M. P. Spector.** 2002. Microbial physiology, 4th ed. Wiley-Liss, Inc., New York, NY.
57. **Mongkolsuk, S., and J. D. Helmann.** 2002. Regulation of inducible peroxide stress responses. Mol. Microbiol. **45:**9–15.
58. **Mostertz, J., C. Scharf, M. Hecker, and G. Homuth.** 2004. Transcriptome and proteome analysis of *Bacillus subtilis* gene expression in response to superoxide and peroxide stress. Microbiology **150:**497–512.
59. **Newman, S. L.** 1999. Macrophages in host defense against *Histoplasma capsulatum*. Trends Microbiol. **7:**67–71.
60. **Nunoshiba, T., T. Watanabe, Y. Nakabeppu, and K. Yamamoto.** 2002. Mutagenic target for hydroxyl radicals generated in *Escherichia coli* mutant deficient in Mn- and Fe-superoxide dismutases and Fur, a repressor for iron-uptake systems. DNA Repair (Amsterdam) **1:**411–418.
61. **Ollinger, J., K. B. Song, H. Antelmann, M. Hecker, and J. D. Helmann.** 2006. Role of the Fur regulon in iron transport in *Bacillus subtilis*. J. Bacteriol. **188:**3664–3673.
62. **Passalacqua, K. D., N. H. Bergman, A. Herring-Palmer, and P. Hanna.** 2006. The superoxide dismutases of *Bacillus anthracis* do not cooperatively protect against endogenous superoxide stress. J. Bacteriol. **188:**3837–3848.
63. **Passalacqua, K. D., and N. H. Bergman.** 2006. *Bacillus anthracis*: interactions with the host and establishment of inhalational anthrax. Future Microbiol. **1:**397–415.
64. **Pomposiello, P. J., M. H. Bennik, and B. Demple.** 2001. Genome-wide transcriptional profiling of the *Escherichia coli* responses to superoxide stress and sodium salicylate. J. Bacteriol. **183:**3890–3902.
65. **Pomposiello, P. J., and B. Demple.** 2001. Redox-operated genetic switches: the SoxR and OxyR transcription factors. Trends Biotechnol. **19:**109–114.
66. **Rocha, E. R., T. Selby, J. P. Coleman, and C. J. Smith.** 1996. Oxidative stress response in an anaerobe, *Bacteroides fragilis*: a role for catalase in protection against hydrogen peroxide. J. Bacteriol. **178:**6895–6903.
67. **Rowland, B. M., T. H. Grossman, M. S. Osburne, and H. W. Taber.** 1996. Sequence and genetic organization of a *Bacillus subtilis* operon encoding 2,3-dihydroxybenzoate biosynthetic enzymes. Gene **178:**119–123.
68. **Rychlik, I., and P. A. Barrow.** 2005. *Salmonella* stress management and its relevance to behaviour during intestinal colonisation and infection. FEMS Microbiol. Rev. **29:**1021–1040.
68a. **Saeed, A. I., V. Sharov, J. White, J. Li, W. Liang, N. Bhagabat, J. Braisted, M. Klapa, T. Currier, M. Thiagarajan, A. Sturn, M. Snuffin, A. Rezantsev, D. Popov, A. Ryltsov, E. Kostukovich, I. Borisovsky, Z. Liu, A. Vinsavich, V. Trush, and J. Quackenbush.** 2003. TM4: a free, open-source system for microarray data management and analysis. BioTechniques **34:**374–378.
69. **Salunkhe, P., T. Topfer, J. Buer, and B. Tummler.** 2005. Genome-wide transcriptional profiling of the steady-state response of *Pseudomonas aeruginosa* to hydrogen peroxide. J. Bacteriol. **187:**2565–2572.
70. **Schumann, W.** 2003. The *Bacillus subtilis* heat shock stimulon. Cell Stress Chaperones **8:**207–217.
71. **Shah, S. V.** 2006. Oxidants and iron in progressive kidney disease. J. Ren. Nutr. **16:**185–189.
72. **Smith, M. A.** 2006. Oxidative stress and iron imbalance in Alzheimer disease: how rust became the fuss! J. Alzheimers Dis. **9:**305–308.
73. **Stegmann, E., C. Rausch, S. Stockert, D. Burkert, and W. Wohlleben.** 2006. The small MbtH-like protein encoded by an internal gene of the balhimycin biosynthetic gene cluster is not required for glycopeptide production. FEMS Microbiol. Lett. **262:**85–92.
74. **Sterne, M.** 1939. The immunization of laboratory animals against anthrax. Onderstepoort J. Vet. Sci. Anim. Indust. **13:**313–317.
75. **Sureda, A., U. Hebling, A. Pons, and S. Mueller.** 2005. Extracellular H_2O_2 and not superoxide determines the compartment-specific activation of transferrin receptor by iron regulatory protein 1. Free Radic. Res. **39:**817–824.
76. **Tam, L. T., H. Antelmann, C. Eymann, D. Albrecht, J. Bernhardt, and M. Hecker.** 2006. Proteome signatures for stress and starvation in *Bacillus subtilis* as revealed by a 2-D gel image color coding approach. Proteomics **6:**4565–4585.
77. **Wandersman, C., and P. Delepelaire.** 2004. Bacterial iron sources: from siderophores to hemophores. Annu. Rev. Microbiol. **58:**611–647.
78. **Wang, G., R. C. Conover, A. A. Olczak, P. Alamuri, M. K. Johnson, and R. J. Maier.** 2005. Oxidative stress defense mechanisms to counter iron-promoted DNA damage in *Helicobacter pylori*. Free Radic. Res. **39:**1183–1191.
79. **Wilson, M. K., R. J. Abergel, K. N. Raymond, J. E. Arceneaux, and B. R. Byers.** 2006. Siderophores of *Bacillus anthracis*, *Bacillus cereus*, and *Bacillus thuringiensis*. Biochem. Biophys. Res. Commun. **348:**320–325.
80. **Zeller, T., O. V. Moskvin, K. Li, G. Klug, and M. Gomelsky.** 2005. Transcriptome and physiological responses to hydrogen peroxide of the facultatively phototrophic bacterium *Rhodobacter sphaeroides*. J. Bacteriol. **187:**7232–7242.